Scale-up Parameters for Fuel Cell Catalyst Dispersions and Pilot Scale Layer Formation in indirect Roll-to-Roll Fabrication of Catalyst coated Membranes for Proton Exchange Membrane Fuel Cells

L. Grebener,[1] A. S. Odungat,[1] Y. Zhu,[1] O. Pasdag,[2] S. Heckenbach,[1] A. Kubina,[3] S. Kohsakowski,[3] F. Özcan,[1,4,z] D. Segets[1,4]

[1] Institute for Energy and Material Processes – Particle Science and Technology, University Duisburg-Essen, Duisburg/DE
[2] ZBT GmbH – The Hydrogen and Fuel Cell Center, Duisburg/DE
[3] Laufenberg GmbH, Krefeld/DE
[4] CENIDE – Center for Nanointegration Duisburg-Essen/DE
[z] Corresponding Author fatih.oezcan@uni-due.de

Highlights

- Catalyst coated membranes for proton exchange membrane fuel cells
- Catalyst dispersions, adsorption kinetics, scale-up
- Nanoparticle processing
- Roll-to-roll manufacturing on pilot scale

Abstract

In this work, essential scale-up aspects of the fabrication of catalyst coated membranes (CCMs) for hydrogen fuel cells via the indirect decal process are investigated. In this process, the catalyst powder is dispersed with a binder in a liquid, coated and dried onto a decal foil. Finally, the catalyst layer is transferred by calendering onto the membrane to yield a CCM for the application in hydrogen fuel cells. In the past, experiments along this and competitive process routes focused either on the final catalyst layer, or the experiments have been performed on laboratory scale only. The investigations presented in this work aim to close this research gap: the scale-up of the fabrication and processing of semi-finished goods for the production of CCMs via the indirect decal process. Since the scale-up factors of processes with heterogenous process media (like solid-liquid dispersions) are typically small, experiments on a pilot scale are in place.

In a first step, the adsorption kinetics of the binder onto the catalyst surface are investigated to define the decisive process variables, time and temperature, of the dispersion preparation. Secondly, the agitation mechanics for the non-Newtonian catalyst dispersion are studied in a proper setup and a viable workflow is established. Finally, the layer formation and performance are investigated both on laboratory as well as on pilot scale. With this work, process variables for the production scale fabrication of CCMs are investigated and established.

Formula symbols

Symbol	Unit	Property
a	$\mathrm{Pa \cdot s^b}$	power-law fluid fitting parameter
b	-	power-law fluid fitting exponent
d	m	diameter
C	-	fitting parameter for dimensionless representation
f	-	function, universal
Fr	-	Froude number
i	$\mathrm{A/cm^2}$	Current density
k_1, k_2	$1/\mathrm{min}$	rate constants of adsorption kinetics
m	kg	mass
M	N·m	momentum
n	$1/\mathrm{s}$	rotational frequency
Ne	-	Newton number
P	W	power
Q	kg/kg	adsorption capacity, ionomer/catalyst
Re	-	Reynolds number
R^2	-	Coefficient of determination
Res^2	-	squared residual sum
t	s, min or h	Time
U	V	Electrical potential / voltage
V	$\mathrm{m^3}$	volume
x	m	particle size
Q_3	-	cumulative size distribution by volume

Greek symbols	Unit	Property
β	kg/kg	mass fraction
$\dot{\gamma}$	$1/\mathrm{s}$	shear rate
δ	kg/kg	dilution ratio
ε	-	correction factor
ζ	$\mathrm{m^2/g}$	specific surface area
η	Pa·s	dynamic viscosity
θ	-	adsorption capacity
ρ	$\mathrm{kg/m^3}$	density
τ	$\mathrm{N/m^2 = Pa}$	shear stress

Indices	
a	alcohol
ads	adsorbed
CB	carbon black
$cell$	related to electrochemical cell
$disp$	dispersion
e	equilibrium
$free$	free, not absorbed
$fluid$	intrinsic for the fluid
i	ionomer
$particle$	intrinsic for the particle
t	at time t
tot	total amount
w	water

1. Introduction

The demand for renewable fuels like hydrogen from electrolyzation equally increases the demand for devices to harvest the energy in decentralized infrastructures. Fuel cells (FC) with proton exchange membranes (PEM) are among the most promising devices for future local energy supply, both in stationary and mobile applications. The cells of low temperature hydrogen FCs generally consist of a membrane electrode assembly (MEA) with a gas diffusion layer (GDL) on the outside, and a catalyst layer (CL) on the inside on top of the PEM. Thus, the electrochemical reactions take place in the CLs. While the anode reaction is rated to be comparably fast, the cathode reaction is much more complicated, involving multiple species and transfer of four electrons. Therefore, much of the noble metal catalyst used in the MEA is applied on the cathode side, so that the majority of the costs are driven by the cathode catalyst and the membrane. James et al. [1] analyzed the cost driving factors for the production of fuel cells and found that depending on the production volume, catalyst and membrane make up substantially 44 % to 70 % of the total costs. Yet, if the production can be scaled, the total cost per stack can be lowered by a factor of about 3. Therefore, it is apparent that a scaled production of catalyst components is important for both the implementation and cost effectiveness of hydrogen PEM-FCs with special emphasis on the cathode.

Even though fuel cells are not a new concept, in recent years different approaches have been established to further facilitate a scaled production of fuel cell components, often yet not always by continuous roll-to-roll (R2R) processes. Different techniques are in use to either cast or spray a catalyst dispersion onto the membrane to produce a catalyst coated membrane (CCM) or onto the GDL to produce a gas diffusion electrode (GDE). The techniques involved are ink-jet printing [2, 3] or spray coating [4, 5] with medium to low-viscous dispersions and gravure coating [6] as well as slot-die coating [7–10] accompanied with simulations on the process window for web velocity and dispersion flow [11].

In two previous publications [12, 13] it was shown that another indirect but scalable approach to produce catalyst coated membranes is viable too. The catalyst dispersion is cast on a decal foil, which is then hot-pressed to the membrane transferring the CL. Throughout the study, it became apparent that proper catalyst dispersion formulation and preparation is vital for the success of the process. The formulation of catalyst dispersions for PEM-FCs based on carbon-platinum particles, perfluoro sulfonic acid binder and various solvents has been studied from different perspectives: simulations of the ionomer behavior and its adsorption on carbon surfaces, impact on the viscosity, as well as impact of different solvents or solid content on layer formation [7, 14–27]. In general, it is apparent that catalyst dispersion formulation and fabrication have an impact on the CL formation and FC performance. However, the scale-up of the production of CCMs or GDEs was focused on the area in m^2 of CCM or GDL achieved and the use of therefore appropriate methods, the final product was in focus, less so the intermediate catalyst dispersion. Often, if a new method for scalable or scaled manufacturing is presented, only limited effort is focused on the scaled preparation of catalyst dispersion or its characterization, including abstaining from the use of ultrasound techniques [2–4, 6–8]. Yet, the preceding work [12], however demonstrating the importance of proper dispersion preparation, is no exception to this blind spot and open questions remain regarding the fabrication of larger amounts of catalyst dispersions for PEM-FCs in the process route

presented there. While the preceding publication [13] addressed process variables regarding the layer formation and transfer, open questions on the dispersion formulation involve the following experimental tasks:

- The ideal mixing time and temperature need to be determined based on ionomer adsorption onto the catalyst surface.
- The change from a vial of 20 mL volume with a fast-rotating magnetic stirrer to a tank with an overhead motor requires a proper selection of an agitator to prevent premature sedimentation and agglutination.
- The chemicals cannot be added in arbitrary order, e.g. if the catalyst is added first, suspending it in a liquid is an unreasonable effort on a liter-scale – as the catalyst is stuck on the bottom; adding the catalyst to the pure alcohol is a fire hazard.
- Once the adsorption in a stirred tank is completed, the comminution should be investigated on pilot scale as well with respect to the dispersion and CL quality.

These examples can be generalized to the point that quantitative and qualitative variables need to be set for this process. An overview of the fabrication of CLs for PEM-FCs and the process variables which are to be investigated in this work is presented in Figure 1.

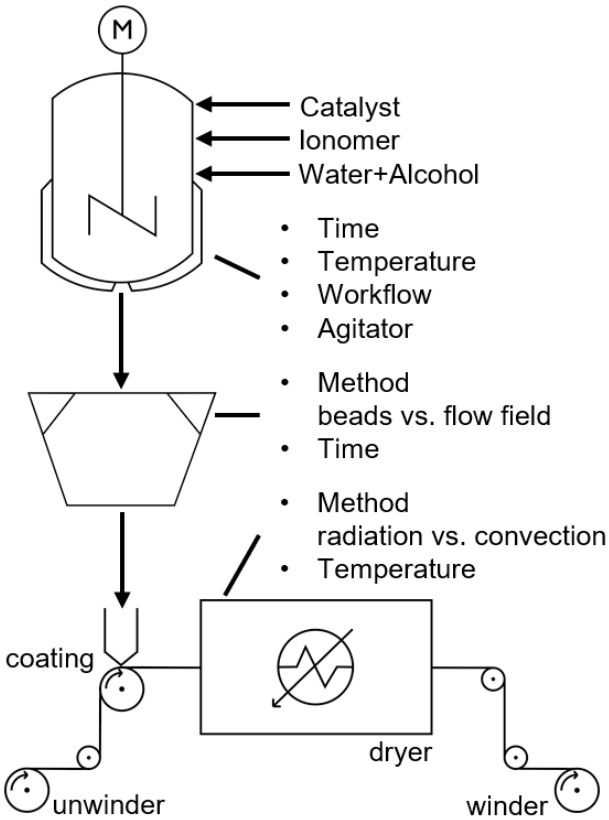

Figure 1 Simplified process flow chart for the fabrication of CLs for PEM-FCs as demonstrated in [12]. The bullet points mark the process variables to be investigated in this work.

Without doubt, these questions and process steps involved are well known in process development. Yet, the scale-up factors for heterogenous unit operations are usually well below those that only involve one fluid phase [28 p. 883ff], predictions and calculations become even more unprecise if non-Newtonian fluids like a catalyst dispersion or other nano materials are involved. A fortiori, this study aims to address these questions and provide criterions as well as insights into scaled process-product relationships for the indirect fabrication route of CCMs.

For these reasons, experiments have been conducted with special emphasis on the scale-up of catalyst dispersion fabrication. The mixing of the components, which is the first operation in Figure 1, is investigated in a first step. The necessary duration and temperature are assessed by determining the ionomer adsorption kinetics. Secondly, the workflow, i.e. in which order the components are added, and the stirring mechanics are examined for different agitator geometries to find suitable equipment for larger scale production.

After these two steps, the comminution is investigated on a laboratory scale by beads milling which have not been covered in the preceding work [12]. The performance of this operation is judged also by the subsequent CL formation, likewise on laboratory scale. This work then concludes with three experiments for the catalyst dispersion preparation and CL formation on pilot scale. To prepare the dispersions, a proper stirring setup was used, that is for the comminution a variation of a high-speed dissolver and a rotor-stator system. Finally, the prepared catalyst dispersions are characterized for their performance in a fuel cell setup under realistic testing conditions.

2. Experimental

2.1 Materials

All chemicals used in this study are commercially available. The materials for the preparation of dispersions are the same as those in the preceding publication [12] except for the ionomers. All chemicals are listed in Table 1. The carbon black (CB) Vulcan XC72R used for the agitation mechanics is chosen for the medium surface area of about 250 m^2/g [29]. The catalyst is technical grade and based on Platinum (about 50 wt% and 5 nm) supported on CB (primary particle size about 30 nm) which forms a complex three-dimensional network. It is described in detail in [12]. The ionomers (perfluorosulfonic acid binders with the properties of solid electrolytes) used in this work are commercially available. However, the sources of catalyst powder and ionomers cannot be disclosed due to legal agreements.

The dispersions are generally formulated for a volumetric ionomer to carbon (I/C) ratio of 0.9, 15 wt% solid content, and a ratio of 30 wt% water and 70 wt% alcohol in the liquid part. If CB is used instead of the catalyst, the corresponding volume was added to the liquids. For the initial coatings, the same decal foil was used as in the preceding study which is a commercially available PET foil with a release liner. This release liner acts as a predetermined breaking point for the catalyst transfer. The catalyst layers are transferred by calendering to a commercial membrane (Fumapem FS-715-RFS), as described in [12].

Table 1 Chemicals used for dispersion preparation.

Chemical	Supplier	Quality / Purity
Platinum on carbon powder, approx. 50 wt% Pt	Commercial	-
Vulcan XC72R	Cabot	-
Ionomer A (IA) in solution	Commercial	-
Ionomer B (IB) in solution	Commercial	-
1-Propanol	VWR	≥ 99.5 %
DI-Water	In house	2.7 µS/cm

2.2 Dispersion characterization

To characterize the different dispersions throughout the study, analytical centrifugation (AC) has been performed (LUMiSizer, LUM) as used by Bapat et al. [30, 31] at 4000 rpm (about 2300 g) and 15 °C. Centrifugations have been performed at both the original concentration to evaluate the stability by so-called transmittograms and at very dilute 0.02 wt% for determining the particle size distribution (PSD) assuming Stokes sedimentation behavior. Dilutions have been made with the water/alcohol mixture (30/70 wt%). Additionally, the flow properties of the dispersions in their original concentration have been characterized with a rheometer (Anton Paar MCR 102) with the CP50-1 cone-plate geometry at 20 °C.

2.3 Adsorption kinetics

To determine the rate of adsorption of ionomer onto the catalyst surface, the catalyst needs to be stirred with the ionomer in the water/alcohol mixture for a determined duration and temperature. The ionomer concentration in either the liquid or solid phase needs to be determined from this original dispersion to quantify the adsorption. Different methods have been used in the past to assess the adsorption isotherm, like ^{19}F NMR [22] and determining the ionomer concentration by the liquid density after centrifugation and filtration [27]. Yet, the original 15 wt% solid content dispersion is often very stable (as append by the results in the later discussion) and cannot be separated even by long centrifugation of > 2 h at 16700 g. Therefore, the procedure is set up to include a dilution step for faster separation within a reasonable time scale (Figure 2):

1. Water, alcohol and ionomer for a dispersion of 10 g total is added to a vial with a stirring bar. The vial is sealed and placed on a hot plate with temperature control.
2. When the designated temperature is reached, the catalyst is added, the vial is sealed again.
3. After the desired time, the vial is removed from the hot-plate and diluted to 1.5 wt% solid content with a water/alcohol mixture (30/70°wt%). Samples with a stirring time of about 48 h are assumed to be in equilibrium state.
4. The sample is centrifuged (Eppendorf Centrifuge 5804) at about 16700 g for 45 min, and the supernatant liquid is collected and filtered through a 0.1 µm syringe filter.

5. The ionomer concentration is determined by gravimetry. The samples are dried on weighing trays under mild conditions of 60 °C and ventilation.

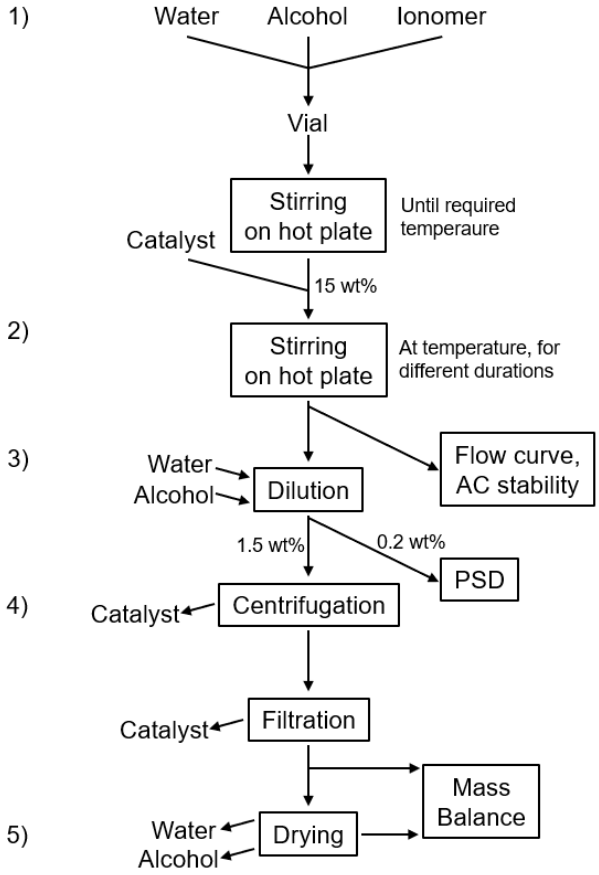

Figure 2 Experimental procedure to investigate the adsorption kinetics of the ionomers by mass balance and the impact on the dispersion properties regarding viscosity, stability and particle size. The numbers on the left refer to the steps described in the text.

Rajupet et al. [32] investigated the impact of the electrostatic repulsion between free and adsorbed ionomer. Combined with apolar interactions, an energy barrier forms for both further adsorption as well as desorption of ionomer. Therefore, the desorption should slow down substantially during the centrifugation. While measuring the concentration of ionomer by the liquid density is very promising (Figure S 1, $R^2 > 0.99$), the final concentration after adsorption and dilution appears to be very small – not to mention inaccuracies from the water/alcohol mixing ratio. Therefore, the measurement of minor density variations appears to be less favorable over an analytical balance and proper drying which is the reason to choose gravimetry in this study. To account for possible systematic errors during the separation (e.g. losses by filtration), one trial was conducted without addition of catalyst powder, so the comparison of the initial and final concentration yields a factor for the correction of other trials. The amount of adsorbed ionomer is calculated from the mass balance, the exact equations are derived in the SI. Additionally, from the dispersion after step 2, samples are taken for characterization by AC (transmittograms and PSD) and rheometer.

2.4 Agitation mechanics

For the agitation experiments, an ordinary laboratory scale glassware setup with an overhead stirrer was used. A cylindrical vessel of 250 mL (internal diameter 63 mm) total volume is attached to a top cover that is held by a stand. This cover is equipped with a reflux condenser, the agitator shaft which can be used with a sealant sleeve, and another opening for the adding of chemicals from the top. The agitator is driven by an overhead stirring motor (Hei-TORQUE Ultimate 200, Heidolph instruments). This motor can display the torque, which is applied to the agitator, yet it should be mentioned that the precision of these values is limited (approx. 0.1 N·cm in best case) and cannot be compared to e.g. a rheometer. Stirring trials have been performed for a turbine stirrer (30 mm diameter), 6-bladed Rushton disk (30 mm), helical ribbon (50 mm, 3 ribbons) and dissolver (42 mm) by varying the rotational frequency and recording the torque. The distance from the bottom of the vessel to the stirrer was kept at about 12 mm, the filling height of the vessel was about 75 mm for 200 mL dispersion/solution.

Trials have been performed for the pure solvent mixture water/alcohol followed by CB in water/alcohol and finally CB in water/alcohol with ionomer IA. CB was used to save on noble metal catalyst and allow for a sufficient number of experiments. In the dispersions, CB was used in the same volumetric concentration as the catalyst would be in the original formulation. Video recording was done with an ordinary phone (Samsung S24) in slow motion mode.

The use of CB instead of the catalyst particles (Pt on CB) bears the risk of performing the experiments with particles which are similar, but not the same as the catalyst. The dispersibility of CB particles is sensitive to its surface properties such as oxidation and specific surface area [29, 33], hence Vulcan XC72R was chosen for being as similar as possible to the commercial catalyst considering the broad range of properties CB particles can have. The omission of platinum is a major simplification, but a necessity due to material availability and prices. Hence it is a strategy chosen on several occasions [16, 21, 23, 26, 34, 35]. However, the results were validated afterwards with the original catalyst for the preparation of CLs on larger scale, using the insights gained with CB.

2.5 Dispersion preparation and layer formation on laboratory scale

In preceding work [12], the dispersion was comminuted in a 10-milliliter-scale rotor-stator system after the stirring period. To explore the viability of different methods to finalize the dispersion by a comminution step for the specific catalyst dispersions used in this study, different methods have been applied. A common method, well-known from paints and varnishes, are beads mills, used in this study on a small scale with an IKA Ultra Turrax tube drive filled with 23 g Cerium stabilized Zirconia beads (Netzsch, CeraBeads, diameter 2.0-2.2 mm, density 6200 kg/m^3). With 10 g of dispersion (density about 935 kg/m^3) added, the volumetric ratio of grinding bodies to dispersion was about 2.9, and the drive was operated for 1 to 20 min for both ionomers with and without a 24 h stirring period at 50 °C, which was performed as described for the adsorption kinetics (2.3).

The CLs are formed by coating the decal foil with the catalyst dispersion. On a small scale (dispersions from beads milling) this is done using a tabletop doctor blade coater (TQC Sheen) with a vacuum and heating plate. The procedure is as described in [12] with the only difference that the liquid film was 100 µm thick instead of 150 µm to account for the higher solid content of the dispersions.

2.6 Strategy and methodology for dispersion preparation and CL formation on pilot scale

Due to limitations on the availability of the precious components (ionomer, catalyst) and the machinery, experiments on a pilot scale could only be performed with a limited number of experimental variations. It is therefore necessary to carefully choose the experiments based on the results of the experiments before on smaller scale and the use of less cost intensive materials. Furthermore, to make the most use of the material available, the experiments are linked in such a manner that more than one process step can be studied from the same batch. Following stirring and comminution, the catalyst dispersions were coated onto the decal foil. For this purpose, a pilot scale R2R machine has been used: Coatema Click&Coat (Model series 11), which is a modular system for continuous coating. The setup included an unwinder, a metered coating section, a drying section as well as rewinder. The web width was about 300 mm. The wet-film thickness was set to be about 100 µm, thus the consumption is about 100 mL/m^2. The web speed was at 1 m/min. This way, the CL can be fabricated as a semifinished product on the transfer foil. With respect to the limitations on material, the following experiments were conducted.

For coating experiments on larger scale, catalyst dispersions have been prepared in the same setup as for the study of the agitation mechanics (2.4). Using the helical ribbon at 180 rpm, ionomer, water and alcohol were added and agitated in this order. Finally, the Pt on CB catalyst was added and submerged by the stirrer, similar to the experiments with CB before. After the addition, the vessel was heated by a kettle with silicone oil on a thermoset (50 °C) hot plate.

1. As one method to comminute a batch of catalyst dispersion a rotor-stator system (Filmix 56-L Primix) was used to grind a dispersion with ionomer IB. This device operates with a high-speed rotor (6500 rpm, 30 m/s), which causes a shear stress over the gap to the stator of about 0.54 mm. The device, though it can be operated continuously in principle, was used in batches of 100 mL to examine different residue times. A cooling jacket prevented overheating. The comminution was carried out for 1 to 5 minutes for prestirred dispersions (24 h, 50°C) and dispersions without stirring (the samples have only been mixed for about 10 min at room temperature to assure an equal distribution of the components). The dispersions were characterized by AC (transmittograms) as well as with the rheometer to determine the flow curves.
   The application coating was done as described with the Click&Coat setup, which was equipped with three convection dryers, each about 1 m long. The temperature was set to 80 °C.

2. Another set of pilot scale experiments were performed starting again with the use of the stirrer setup described in Section 2.4. The dispersion was stirred for about 3 h at 50 °C, using the results of the adsorption study from Section 2.3 which have been acquired in the meantime.
   For comminution, another device which functions on the basis of shear gradients is the dissolver, similar to the agitator used by the agitation mechanics section, only at a much

higher rotation frequency. Using the same glass vessel as for the agitation and thus avoiding transfer, 200 mL catalyst dispersion with ionomer IA have been comminuted with a dissolver (Erichsen Dissolver 492 I, 40 mm diameter) at 1500 rpm for 10 and 20 min. For a suited dispersion and geometry, a flow will set in above and below the fast-rotating dissolver blade. The rotation frequency was chosen according to the desired flow patterns (so called doughnut flow patterns). For a high viscous shear-thinning fluid, a strong shear stress occurs, as the shear gradient would reach out less than for low-viscous Newtonian fluids.

Like before, the dispersions were characterized with AC and rheometer. The coating was performed with another Coatema setup similar to before, only the dryer was now a single infrared drying unit, set to 90 °C.

3. Finally, the last experiment was performed on pilot scale under consideration of the results of the two former approaches. The stirring was performed like in experiment 2 with 3 h at 50 °C using ionomer IA. The comminution was done with the Filmix from experiment 1 and equal settings for 5 min. Coatings of the catalyst dispersion on the transfer foil were done with the setup including the infrared dryer.

2.7 Catalyst layer characterization, transfer and electrochemical evaluation

To characterize the CLs as a measure for the success of the comminution and coating operation, microscopy was used (Olympus BX51) as well as optical profilometry for three-dimensional imaging (S Neox 090 in confocal mode). The CLs were transferred as described in [12], similarly the electrochemical performance was evaluated as explained in detail before [12]. The CL is transferred to a membrane by hot-pressing yielding a sample of about 6.5 by 6.5 cm. This CCM is then characterized in a test setup designed to mirror realistic operational conditions, such as 70 % relative humidity and a temperature of 80 °C.

3. Results and Discussion

The discussion of the results follows the process flow and the process variables to be investigated as presented in Figure 1. The presentation is structured just like the process flow, i.e., starting with the agitation and the process setup prior shifting to the comminution. While for the agitation, the dispersion properties are investigated, investigations on the comminution also involve the layer formation to judge the viability on the quality of the CLs as well.

3.1 Adsorption kinetics

The adsorption behavior of ionomers onto the surface of CB and related catalyst for fuel cells have been studied in the past [22, 23, 27, 36–39]. Typically, the focus is on adsorption isotherms, describing the dispersion in equilibrium state. Yet, for the fabrication of catalyst dispersions it is not economically reasonable to wait until equilibrium has been achieved – theoretically an infinite time. Therefore, to determine recommendable time and temperature values for the stirring process, the adsorption kinetic needs to be studied. Simplified approaches, which summarize diffusion and surface processes, describe the reaction rate to

depend on the difference of the amount of adsorbate at a given time and the equilibrium amount. Different models have been applied to describe the micro-kinetics of adsorption onto CB surfaces, e.g. for waste water treatment [40, 41]. Among them, pseudo-first order and pseudo-second order have been shown to be useful for CB surfaces:

Pseudo-first order (PFO):

$$\frac{d\theta_t}{dt} = k_1(\theta_e - \theta_t) \Rightarrow ln(\theta_e - \theta_t) = ln\theta_e - \theta_1 t \qquad \text{Equation 1}$$

Pseudo-second order (PSO):

$$\frac{d\theta_t}{dt} = k_2(\theta_e - \theta_t)^2 \Rightarrow \frac{t}{\theta_t} = \frac{1}{k_2\theta_e^2} + \frac{t}{\theta_e} \qquad \text{Equation 2}$$

The results of the adsorption study are presented in Figure 3. Panel a) shows the adsorption progression vs. stirring time. The degree of adsorption $\boldsymbol{m_{ads}/m_{tot}}$ is calculated by the amount of ionomer adsorbed divided by the total amount of ionomer in the formulation. In panel b) the adsorption rates calculated from the amount of adsorbed ionomer per catalyst surface area $\boldsymbol{\zeta}$ (about 357 m^2/g [12]) and per amount of suspension $\boldsymbol{m_{disp}}$ are presented. For both ionomers, a strong dependency on the temperature is indicated. At 30 °C, the total amount adsorbed is limited to about 10 to 20 %, with IA still adsorbing to a larger amount after 48 h of about 40%. For 50 °C, the velocity is increased for IA, but almost not significantly for IB. Both ionomers reach close-to-equilibrium state in about 2 h, but IA is at about 70°% adsorbed ionomer and IB at about 30 %. Yet increasing the temperature further complicates the matter. From the handling of ionomer solutions for membranes, it is known that depending on the conditions the ionomer forms a high-viscous gel [42–44]. At elevated temperatures, this is true for the catalyst dispersions as well. Figure S 2 displays the flow curves of the catalyst dispersions from Figure 3 for the duration of 0.5 to 2 h and 30 to 70 °C as well as the initial viscosity.

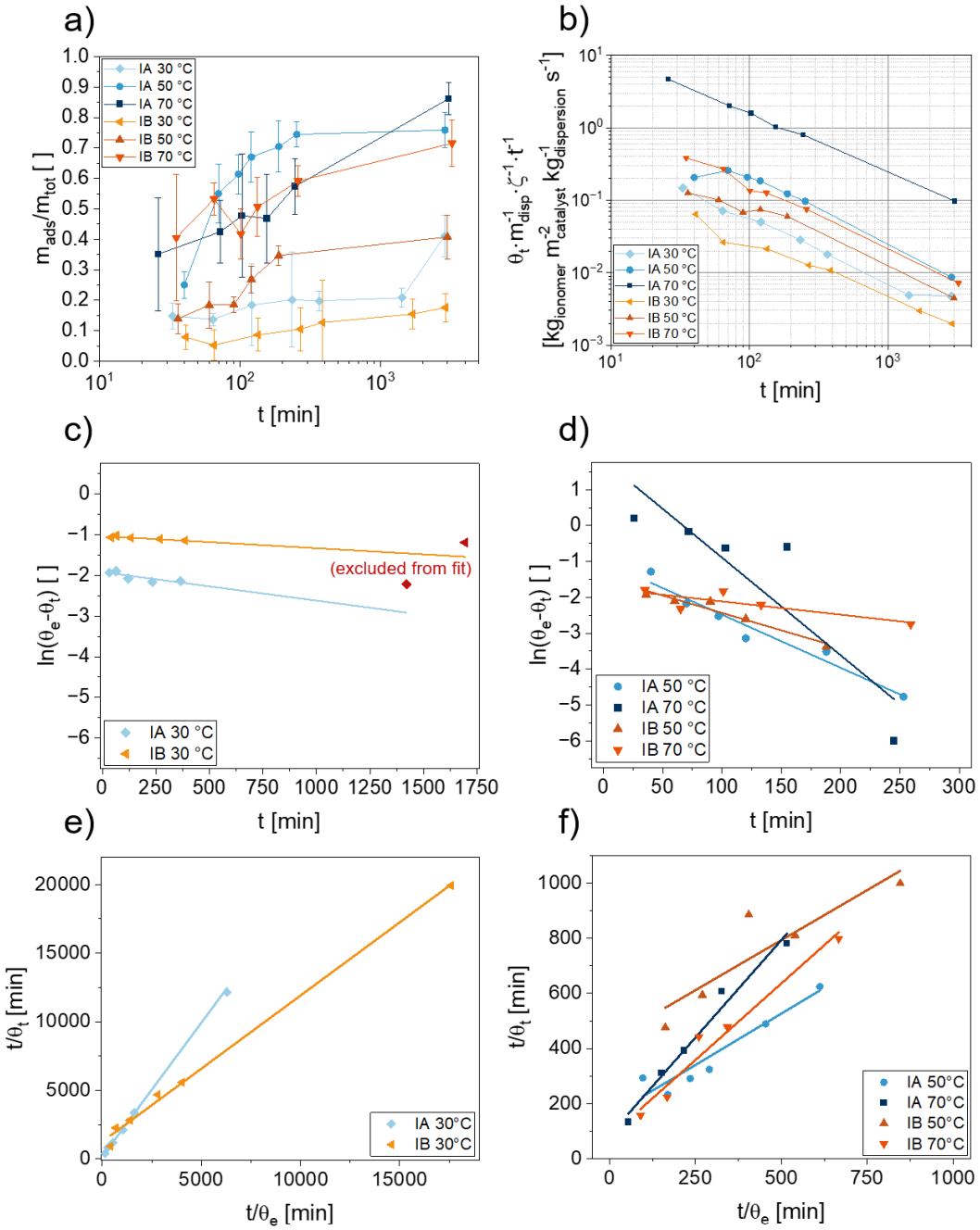

Figure 3 Kinetics of the ionomers adsorbing onto the catalyst surface at temperatures from 30 to 70 °C. a) Saturation of the catalyst surface over time, the degree of adsorption is the amount of adsorbed ionomer relative to the total added ionomer; b) the mean adsorption rate of the ionomer at a given time, averaged from the start to the point in time; c+d) kinetic evaluation by pseudo-first order kinetics; e+f) kinetic evaluation by pseudo-second order kinetics. The red datapoints in c) are excluded from the fitting.

For IA the viscosity increases at 70 °C slowly but is unmeasurably high after two days (not shown in the diagram). The high initial adsorption speed (Figure 3b) of the dispersions at 70 °C is due to the low initial viscosity. But unlike for 50 °C, equilibrium is not reached by 2 h likely due to the gelation beginning to raise the diffusion resistance. On the other hand, the viscosity is lower for the dispersion with IB at 70 °C after 0.5 and 2 h, and the adsorption rate and amount are higher than for the same sample at 50 °C, further indicating the diffusion hinderance by high viscosity. The gelation after 48 h and more can be measured for this sample with a viscosity at low shear rates of > 10^4 Pa·s, which is figuratively jelly-like.

The adsorption of the ionomer is evaluated by the kinetic models PFO (Figure 3 c+d) and PSO (e+f). The fitting parameters are summarized in Table 2. From the results, it is apparent that the fitting by PSO is best for 30 and 70 °C, especially for the later datapoints > 1000 min which are not represented well (c+e). The results at 50 °C on the other hand, are best described by PFO kinetics (d).

Table 2 Fitting parameters for kinetic modelling for ionomer adsorption.

Ionomer type	Temperature	First order kinetics		Second order kinetics	
		k_1	R^2	k_2	R^2
	°C	1/min		1/min	
Ionomer IA	30	0.0007	0.705	0.0916	0.999
	50	0.0148	0.955	0.0401	0.910
	70	0.0272	0.791	0.0511	0.976
Ionomer IB	30	0.0003	0.835	0.0852	0.996
	50	0.0097	0.947	0.0471	0.813
	70	0.0037	0.665	0.0818	0.967

While PFO and PSO summarize the different mass-transport steps (bulk diffusion, pore diffusion, adsorption), the two approaches are generally interpreted to indicate different conditions: for PFO the concentration of adsorbate is high compared to the number of active sites on the adsorbent, for PSO it is vice versa. [40] This can have different reasons. In the case of this study, where the concentration of both is nominally constant, it is probably due to the difference of diffusion velocity and the adsorption micro-kinetics (i.e. the elemental adsorption reaction). It can be concluded thus that at 30 °C, adsorption is limited by the diffusion velocity at this low temperature, at 50 °C by the adsorption step itself is limiting, and at 70 °C the increasing viscosity caused by the gelation limits the diffusion and therefore the adsorption overall.

To evaluate the stirred but not comminuted catalyst dispersion as a central intermediate product in this process, AC measurements were carried out. The Stokes equivalent PSDs are presented in Figure S 3, while the transmittograms which show the stability of the dispersion at 15 wt% concentration are displayed in Figure S 4 and Figure S 5. In summary, the particle size of the dispersions with IA depends strongly on the duration of mixing at temperatures of 30 and 50 °C, however for 70 °C the particle size does not depend on the stirring time anymore. For IB, the PSDs are narrow and largely independent from the stirring time, which indicates

that not only the adsorption happens differently, but it also results in catalyst dispersions with different properties. The transmittograms indicate that for both ionomers, 30 °C is not sufficient to prepare a stable dispersion, but at 50 °C, stable dispersions are achieved by 0.5 h for IA and 2 h for IB. Finally, for 70 °C IB the dispersion is stable after 2 h of agitation, while the sample after 0.5 h is surprisingly unstable, like the 0 h sample.

From these investigations, the first decisions for process variables can be made: duration and temperature for the stirred catalyst dispersion. As can be seen, for both ionomers the particle size is reduced significantly from the original agglomerate size of the catalyst powder (> 500 nm for the mean particle size [12]). Furthermore, stability and viscosity are most favorable for suspensions of 2 h stirring at 50 °C for IB, while 0.5 h are sufficient for IA. Therefore, the agitation should be set for at least 2 h at 50 °C. Temperatures of 30 °C and below should be avoided for the limited adsorption and stability of the dispersion, as well as high temperatures like 70 °C should not be applied to avoid gelation, especially over longer periods of time (e.g. 24 h or longer).

3.2 Agitation Mechanics

With the adsorption kinetics explored and the duration and temperature during the stirring operation determined, the practical implementation is to be set up. The requirements on this process step are:

- Uncomplicated and safe handling of chemicals
- Mixing of liquids
- Wetting and submersion of the catalyst powder
- Dispersing the catalyst powder to avoid agglutination
- Prevention of sedimentation
- Heating towards the desired temperature

An established unit operation is stirring in a cylindrical vessel, which is able to satisfy all these requirements – unbaffled to avoid caking. However, investigations on the preparation of catalyst dispersions for PEM-FCs using this method have not been reported yet. It should furthermore be noted that the catalyst particles are nanostructured, thus surficial processes might be amplified. To determine the missing process variables, some experiments are in place involving the questions on the order of adding chemicals, the agitator geometry and rotation speed. To determine the order of addition for the chemicals, some variances can be excluded from the beginning. If the catalyst is in contact with undiluted alcohol, a high risk of fire from the reaction of oxidized platinum and alcohol is imminent. Furthermore, if the catalyst is added first and the liquids on top of it, agglutination is certain due to air entrainment and since the solid fraction on the bottom of the vessel is very high, the viscosity is very large as well. The consequence is that the stirrer would be unable to raise the solids and the process fails. Therefore, at least water should be added first.

This was done for a turbine stirrer: 1 g of CB was added slowly to 200 mL of water (see video shots and photographs shown in Figure S 6). The CB is floating on top of the liquid for Re from 2000 to 5000 (viscosity and density with respect to the pure liquid). Only if the stirring is so vigorous that the vortex reaches the turbine and air is entrained (Re = 6000), some of

the CB is submerged and spread in the liquid, yet most of the CB remains undispersed floating on the top. Therefore, the catalyst powder needs to be added to a wetting liquid, at least the water and alcohol. Since the ionomer helps stabilizing the catalyst powder and often arrives as a dry powder, it can be argued to add it prior to the catalyst. Suggestable orders for adding the chemicals therefore are all variations in which the catalyst is added the latest.

To select a proper agitator, different geometries were used. While tangential flow cannot counteract sedimentation, axial and radial flow stirrers are appropriate. Furthermore, agitators can be distinguished for their size with respect to the vessel's diameter, either they are small in diameter and typically rotate at higher frequencies, or vice versa. A major challenge any stirrer geometry needs to address is the change in viscosity. First the liquid starts out water-like, but as the particles are added viscosity can rise over several orders of magnitude, only to possibly fall again as adsorption progresses. The different agitators are turbine stirrer, helical ribbon, Rushton disc (6-bladed), and dissolver.

To describe the physics of a process for upscaling, approaches with dimensionless numbers have been proven useful. For solid-in-liquid dispersions as in this study, a function of Re and Fr can be used to describe Ne [45 p. 212-217]:

$$Ne = f(Re, Fr) \qquad \text{Equation 3}$$

With:

$$Ne = \frac{P}{\rho_{disp} n^3 d^5} = \frac{2\pi n M}{\rho_{disp} n^3 d^5} \qquad \text{Equation 4}$$

$$Re = \frac{\rho_{disp} n d^2}{\eta} \qquad \text{Equation 5}$$

$$Fr = \frac{n^2 d}{g} \cdot \frac{\rho_{disp}}{\rho_{particle} - \rho_{fluid}} \qquad \text{Equation 6}$$

The Newton number is calculated from the driving power of the stirrer, which is derived from the momentum: $P = 2\pi n M$. The Froude number is adjusted to take the particle swarm sedimentation into account, therefore it is extended with the density simplex $\rho_{disp}/\Delta\rho$. Sometimes the Archimedes number is used instead [45 p. xviii]. The Reynolds number depends on the dynamic viscosity η. While this is uncomplicated to determine for a Newtonian liquid, for shear-thinning liquids like in this study, the viscosity is a function of the shear rate $\dot{\gamma}$, which itself depends on the agitator geometry and rotational speed. The determination of the effective viscosity in such a complex scenario has been a challenge for the last decades and addressed in several cases. One procedure is developed on polymer solutions by Metzner and Otto [46] and generalized by Rieger and Novák [47], the latter is used in this study. To apply it to the CB dispersions used in the stirring experiments, the flow curve needs to be described by a power law. In Figure S 7, the flow curve of the dispersion of water, alcohol and CB is shown. The data suggests that the Ostwald-de Waele power law applies [45 p. 51-55]:

$$\tau = a\dot{\gamma}^b \Rightarrow \eta = ab\dot{\gamma}^{b-1} \Rightarrow log(\eta) = log(ab) + (b-1) \cdot log(\dot{\gamma}) \qquad \text{Equation 7}$$

With $b \cong 0.12$ the dispersion is shear-thinning (pseudoplastic). The Rieger-Novák procedure can now be applied with the following steps:

1. Determine $Ne_{w,a,CB} = f(n)$ for the shear-thinning fluid (water-alcohol-CB)
2. Determine $Ne_{w,a} = f(n)$ and $Re_{w,a}$ for the Newtonian fluid (water-alcohol, $\eta_{w,a} = 2.592$ mPa·s at 25 °C) [48]
3. Calculate $Ne_{w,a} = f\left(Re_{w,a}\right)$
4. Calculate the effective $Re'_{w,a,CB} = f^{-1}\left(Ne_{w,a,CB}\right)$ from the function f determined in step number 3
5. Calculate the effective dynamic viscosity $\eta'_{w,a,CB}$ from $Re'_{w,a,CB} = f(n)$
6. Calculate $\eta'_{w,a,CB}$ as a function of n
7. Repeat the steps 1.-6. for the water-alcohol-ionomer-CB dispersion.

Finally, $\eta'_{w,a,CB} = f(n)$ and $\eta'_{w,a,i,CB} = f(n)$ respectively can be used to calculate Re from Equation 5 and with it, $Ne = f(Re, Fr)$. The density of a dispersion ρ_{disp} is approximated from the density of the components, neglecting non-ideal mixture phenomena for all components but water and alcohol ($\rho_{w,a} = 864\ kg/m^3$; $\rho_{CB} = 1800\ kg/m^3$) [48]:

$$\rho_{w,a,CB} \cong \frac{m_{w,a} + m_{CB}}{{m_{w,a}}/{\rho_{w,a}} + {m_{CB}}/{\rho_{CB}}} = 889\frac{kg}{m^3} \qquad \text{Equation 8}$$

And for the dispersion including the ionomer ($\rho_i = 2100\ kg/m^3$) [49]:

$$\rho_{w,a,i,CB} \cong \frac{m_{w,a} + m_i + m_{CB}}{{m_{w,a}}/{\rho_{w,a}} + {m_i}/{\rho_i} + {m_{CB}}/{\rho_{CB}}} = 919\frac{kg}{m^3} \qquad \text{Equation 9}$$

Observations are split into three stages: first the powder being added to the liquid, then all powder added but without the ionomer, and finally the dispersion with ionomer. The initial step involving the wetting of the powder can be observed visually, using a camera in slow motion (about 1/8th of the real speed). Photographs for each stirrer are presented in Figure 4. The second stage is represented by the criterion numbers in Figure 5, and the third stage is represented by Figure 6.

Generally, the observations show that all agitators are able to cause sufficient convection to submerge the particles at moderate turbulence of about $Re_{w/a} = 2500$ (Figure 6 a, c, e, g). The particles are pulled downwards in spirals along the agitator shaft, and as soon as the agitator hits the particles, they spread out into the liquid. Since the agitator of the helical ribbon is larger than the others, the particles are spread earlier. The differences between the agitators are subtle, yet the remobilization of particles from the bottom of the vessel can be observed until the light absorption of the dispersed CB is too high. Here, the effectiveness can be ordered as: turbine stirrer < Rushton disk ≈ dissolver < helical ribbon. Apparently, the high local convection of the smaller agitators like the turbine stirrer translates less into the liquid to raise the particles, even while the viscosity is still low and Newtonian (water-alcohol-ionomer solution).

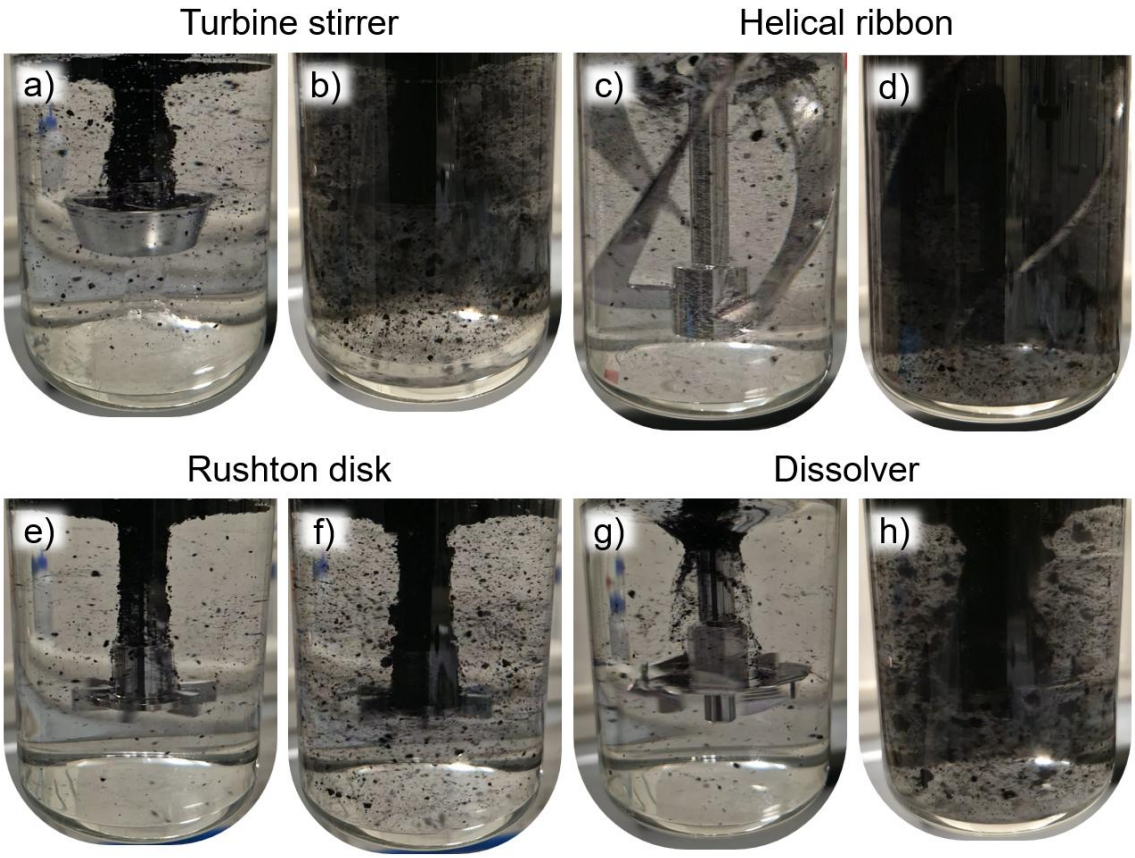

Figure 4 Initial wetting of CB in water, alcohol and ionomer. The images are taken from slow-motion videos while adding the first gram of carbon. The Reynolds numbers are calculated with the density and viscosity of the pure liquid, the stirrers move clockwise. a+b) turbine stirrer at 500 min^{-1} and Re = 2500, c+d) helical ribbon at 180 min^{-1} and Re = 2500, e+f) Rushton disk at 500 min^{-1} and Re = 2500, g+h) dissolver at 250 min^{-1} and Re = 2500.

The further progression of this process can be seen in Figure 5 and Figure 6. Panel a) in each figure shows the three-dimensional representation of the dimensionless numbers from Equation 4 to Equation 6 recorded with all CB added. The diagrams b-d) in Figure 5 and Figure 6 show the two-dimensional projections of pairs of dimensionless numbers. The lines drawn in the diagrams are fittings from the experimental data. To fit the data, an extended power product is used:

$$Ne = C_1 \cdot Re^{C_2} \cdot Fr^{C_3} + C_4 \qquad \text{Equation 10}$$

The parameter C_4 is added to avoid unpractical large values of C_1, which also led to very small values for C_2 and C_3 during optimization. The drawback of introducing such an additive parameter is that handy methods like multiple linear fittings of the logarithmic Ne by matrix operation e.g. in MS Excel cannot be used anymore. Therefore, a simple particle swarm simulation in Python (3.11.11; Spyder IDE v6.0.4) has been used to minimize the sum of the squared residuals of the logarithmic Ne, such that the minimum of Equation 11 is to be found. The use of the logarithmic Ne instead of Ne itself is reasonable with the multiplicative nature of the dimensionless numbers. Otherwise, the minor parts with larger values of Ne would be

emphasized and other parts misrepresented by the fitting function.

$$Res^2 = \sum \left(log(Ne_{measured}) - log(Ne_{calculated}) \right)^2 \qquad \text{Equation 11}$$

The fitting parameters for the criterion of Equation 10 are listed in Table 3. The fitting process was successful in that regard that the functions are able to represent the data with good precision as apparent by the residual sum and the diagrams in Figure 5 and Figure 6. For a Re of 2500, as used in Figure 4, the other dimensionless numbers Fr and Ne are determined and represented in Table 4. From this, the volumetric power density $P/V_{w,a}$ as the scale-up criterion [45 p. 217, p. 231] can be determined from the Newton number and the volume of about 200 mL and compared for the different agitators.

Table 3 Fitting parameters for the dimensionless representation of the agitation of CB dispersions with the squared residuals sum $\boldsymbol{Res^2}$.

Water-alcohol + CB	C_1	C_2	C_3	C_4	Res^2
Turbine stirrer	24.02	-0.22	-0.76	3.53	0.103
Helical ribbon	95.79	-0.45	-0.44	0	0.035
Rushton disk	34.09	-0.19	-0.77	6.97	0.024
Dissolver	645.73	-0.71	-0.55	0.91	0.141
Water-alcohol + CB + Ionomer					
Turbine stirrer	19.10	-0.30	-0.94	3.45	0.353
Helical ribbon	36993.20	-1.22	-0.22	0.90	0.107
Rushton disk	23.85	-0.34	-0.91	5.09	0.092
Dissolver	942.03	-0.71	-0.44	0.57	0.447

These numbers suggest that the helical ribbon requires the least energy to suspend the catalyst particles. Furthermore, as it is larger in diameter it can handle changes in viscosity better than stirrers with a smaller agitator. This circumstance becomes even more relevant for non-Newtonian shear-thinning fluids, for which the decay of shear rate and stress is emphasized. Therefore, the helical ribbon can be suggested as viable agitator geometry.

The experience gained through these experiments with CB can be applied directly. In Section 3.4, experiments on larger scale to prepare 200 mL catalyst dispersions are discussed with the same setup but using Pt on CB catalyst powder instead of Vulcan CB. The above findings have been applied using the helical ribbon at 180 rpm. The handling of the catalyst powder was with less effort than Vulcan CB, as the free-flowing properties are more advantageous, and the powder is less aggregated and as such submerged faster yet in similar patterns.

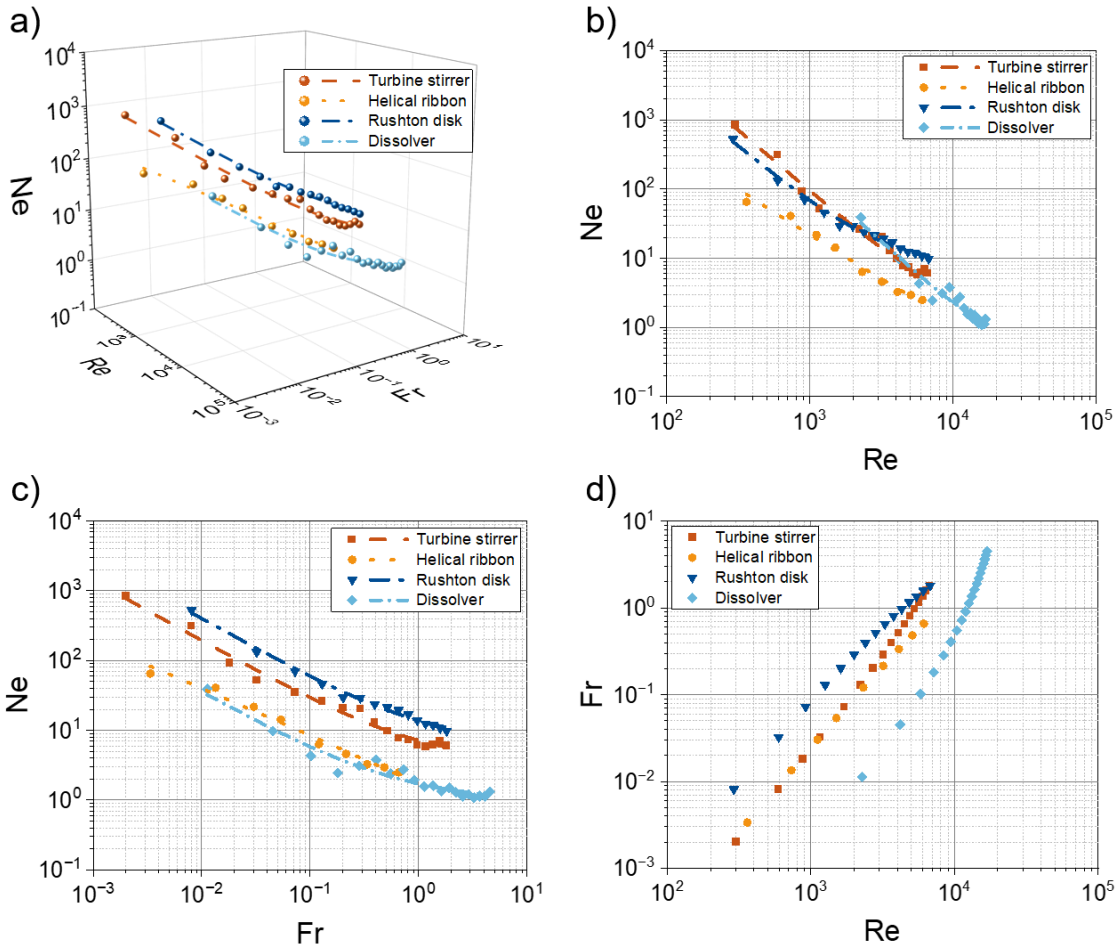

Figure 5 Scale-up parameters for the dispersion of CB in water and alcohol with Ne, Re and Fr. a) Three-dimensional representation, b) projection on Ne vs. Re, c) Ne vs. Fr, d) Fr vs. Re respectively.

Table 4 Volumetric power density and dimensionless parameters as scale-up criterions.

Water-alcohol + CB	Ne	Re	Fr	$P/V_{w,a}$ in kW/m^3
Turbine stirrer	19.34	2500	0.18	1.21
Helical ribbon	6.95	2500	0.13	0.26
Rushton disk	22.89	2500	0.39	1.43
Dissolver	34.23	2500	0.009	1.44
Water-alcohol + CB + Ionomer				
Turbine stirrer	16.78	2500	0.13	1.08
Helical ribbon	6.27	2500	0.04	0.24
Rushton disk	15.07	2500	0.14	0.97
Dissolver	23.69	2500	0.015	1.02

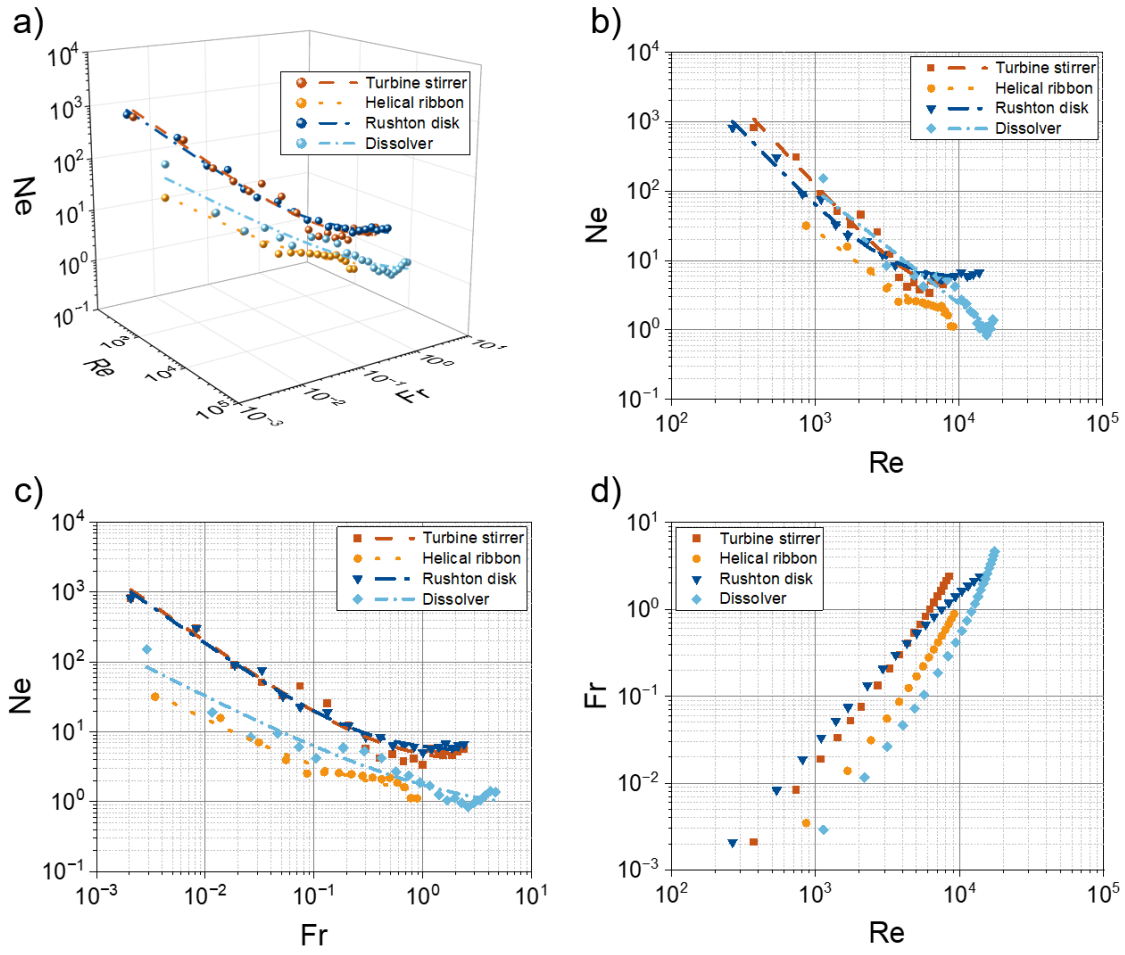

Figure 6 Criterion for the dispersion of CB in water, alcohol and ionomer with Ne, Re and Fr. a) Three-dimensional representation; b) projection on Ne vs. Re; c) Ne vs. Fr; d) Fr vs. Re respectively.

3.3 Catalyst dispersions and layers on laboratory scale

In parallel to the investigation of the stirring process step, the consecutive comminution of the catalyst dispersions was examined. However, in general the scaling of a comminution process can be more complex than of a stirring process but has a large impact on the film formation and coating quality. For this reason, the process will be evaluated from the perspective of the product quality: the dispersion (stability and flow curve) as well as the CL formation (micrographs, profilometry). Desirable properties for the dispersion are a high stability against sedimentation as well as a rather low viscosity. While a high viscosity may lead to problems in film formation and handling, a dispersion with a too low viscosity will face run-off problems from the web during R2R coating. Both can be assessed with the examination of the CLs, e.g. with micrographs.

Dispersions with both different ionomers have been prepared by stirring for either 24 h at 50 °C or for 0 h by adding the components directly to the IKA tube. The PSDs of the dispersions are presented in Figure 7 a+b. They show that the PSDs for both formulations with either ionomer IA or IB are practically identical. The same is the case for the comminution duration. The only influencing factor is, whether there was a 24 h stirring period or not, which lowers the particle size with a factor of about 2. Compared to the PSDs from Figure S 3 c+d (PSD of the dispersions from the adsorption study), it can be seen the change for ionomer IB

is limited, while that for ionomer IA is quite significant as larger agglomerates are broken up. A further drop of the minimal particle size cannot be seen in either case, which indicates that the primary particle size is of about 10 to 30 nm. This is in good agreement with previous results [12].

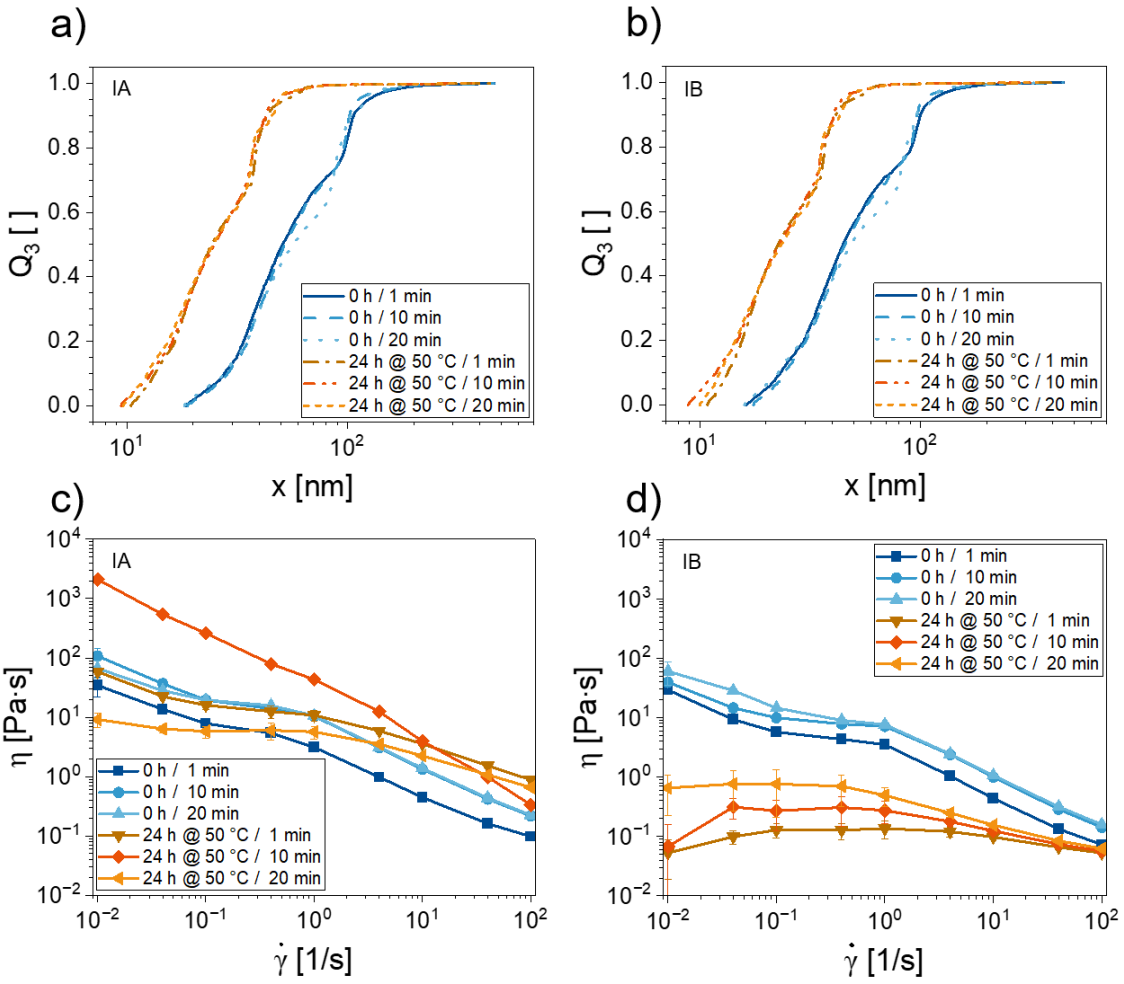

Figure 7 Dispersion characterization of catalyst dispersions from beads milling. The first number of the sample labeling refers to the stirring duration in hours, the second to the comminution duration in minutes in the form of beads milling. a) PSDs of dispersions made with ionomer IA, b) with ionomer IB, c) flow curves of dispersions made with ionomer IA, d) with ionomer IB.

The flow curves of the prepared catalyst dispersions are shown in Figure 7 c+d. The general picture for the formulations with ionomer IA is ambiguous. But for ionomer IB a clear trend can be seen, the low shear rate viscosity is lower by about one to two decades with the stirring period compared to without it and the comminution time increases the viscosity slightly. For ionomer IA without the stirring period, the viscosity increases slightly if the comminution time is increased. If the stirring period is added, the viscosity increases sharply from 1 to 10 min comminution time, only to fall again after 20 min. AC measurements have also been conducted. The transmittograms are presented in Figure S 8. They show that the stability does not depend strongly on the comminution time, but on the type of ionomer and the presence of a stirring period. The highest stability was achieved by dispersions with ionomer IA and with

the stirring period. Independent from the comminution time no sedimentation can be identified. Visible but delayed sedimentation can be seen for the dispersions with ionomer IB with the stirring period. The dispersions are unstable if the stirring period is not applied independent from the ionomer. Noteworthy, the viscosity is not the determining factor for the stability, as dispersions with higher viscosity can sediment faster as in the case of ionomer IB with and without the stirring period.

The results of the ionomer and stirring period on the formation of the CL were studied by optical microscopy and profilometry (Figure S 9 and Figure S 10). Larger agglomerates (several 10s – 100s µm) can, additionally to hindering the transfer of the catalyst layer to the membrane, trigger the formation of cracks within the coating, since the critical film thickness is exceeded locally [50, 51]. These defects cannot be cured later in the transfer from the decal foil to the membrane [13] and are therefore an indicator for a diminished quality as there is the danger of oxygen leaking into the hydrogen stream and vice versa, posing both a lower efficiency as well as a safety risk. Minimizing these cracks and similar gaps in the coating is therefore a quality demand and a micrograph without defects and larger agglomerates is a desirable outcome.

The micrographs (Figure S 9 and Figure S 10) show that only one minute of comminution is too short for a uniform coating with large agglomerates of > 100 µm diameter and cracks around them. These agglomerates have not been apparent before in the PSDs (Figure 6 a+b). This might be due to the sample preparation: the PSDs are recorded from dilute dispersion to be able to apply both Stokes' sedimentation and Lambert-Beer law. Possibly, these large agglomerates > 100 µm sediment too fast to be recorded within the necessary timeframe. However, a much more uniform coating can be achieved with 10 min of comminution. Increasing this duration to 20 min generates only minor changes in the general picture. Under 50x magnification, minor cracks can be identified for the coating of IB with the stirring period and 20 min of comminution. Also, some depressions in the coating of IA under the same conditions are apparent. While the cracks appear during the drying step [12], the origin of the depressions is unclear. It is possible that these occur after some agglomerates with lesser adhesion broke off from the catalyst layer.

Summarizing the results, an adequate stirring period is vital to fabricate stable catalyst dispersions even if comminution is considered. Furthermore, comminution with beads mills should have residue times of about 10 min, to break agglomerates efficiently and yield a homogenous catalyst layer after coating. However, a longer duration such as 20 min might be required to yield a dispersion with reasonable viscosity.

3.4 Catalyst dispersions and layers on pilot scale

In order to investigate the formation of the catalyst layer on a larger scale, a selection of process conditions was made. Following the experiments as described in Chapter 2.6, the feasibility of the indirect fabrication of CCMs is explored on pilot scale. It should be noted that the material constraints led to the necessity to change more than one process parameter at once. Nonetheless, conclusions can be drawn from careful observations.

3.4.1 Experiment 1: Filmix and Convection Dryer

Dispersions were prepared with variations on the stirring period and the comminution duration. Two samples without a prolonged stirring period and four with a stirring period of about 24 h at 50 °C were produced. The comminution with the Filmix was done for individual samples for 1 to 5 min. The dispersions were characterized by AC, the transmittograms are compiled in Figure S 11. In general, the stability is limited for the samples without the prolonged stirring and can be improved for the other samples. The duration of the comminution does not have a significant impact. Additional rheometric experiments have been conducted to determine the flow curves of the dispersions. The results are presented in Figure 8. Both dispersions prepared without the stirring period exhibit a shear-thinning behavior. The sample with 5 min comminution yielding a larger viscosity, about 10 times larger in the low-shear regime, than the 1 min sample. However, the samples with the longer stirring period at 50 °C are not shear-thinning. This is in line with the results from the dispersion on the smaller scale (Figure 7d) as well as from the preceding work [12].

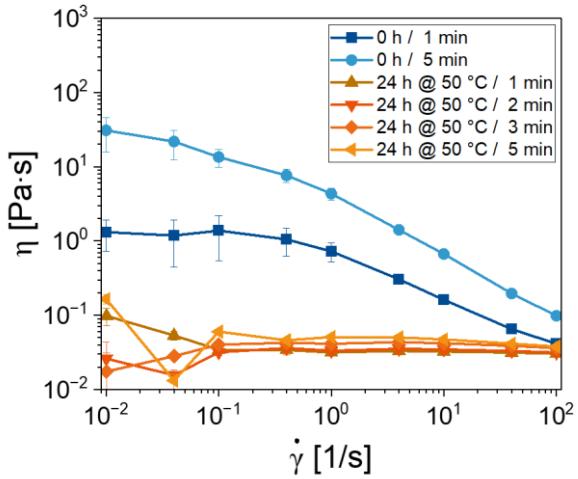

Figure 8 Dispersion characterization of catalyst dispersions from for the large batch Experiment 1 prepared with the Filmix. The data sets labeled “0 h” were prepared with only a brief stirring time of about 10 min at room temperature. The other samples are stirred for about one day at 50 °C. The second number of the labels indicate the comminution time.

It is therefore apparent that for dispersions prepared on this pilot scale there are two decisive properties, sedimentation stability and flow behavior that are comparable to those of dispersions prepared on a smaller scale. This cannot be assumed without experimental confirmation.

The CL prepared from these dispersions including one sample prepared just with stirring and without comminution were characterized by optical microscopy and profilometry. The micrographs are presented in Figure S 12 and Figure S 13. As found before for direct drying on a hot-plate [12], larger agglomerates in the size of several 10s and 100s of micrometers can induce cracks and other defects in the coating. On direct comparison, the agglomerates can be reduced in size as compared to the results on smaller scale. Nonetheless, without the stirring period, the agglomerates induce cracks in the coating, thus the stirring period is necessary in order to reduce the agglomerate size and ensure a more homogeneous CL. The impact of the comminution is to further reduce the agglomerate size from 1 to 5 min, but also to limit the formation of some cavities which seem to form as elongated cracks.

During the application of the catalyst dispersion in the coating of the decal foil a lot of the dispersion ended up running off the applicator roll through the coating unit retrograde to the web motion in the case of the stirred samples (24 h @ 50 °C). Apparently the selected 1 m/s (which was limited by the drying section and partly due to the machinery) is too slow for the liquid. Although this problem can be solved technologically (the run-off liquid can be collected and pumped in cycle), the liquid film is in danger to be below the desired film thickness.

In summary, from this first assessment on pilot scale already some challenges are apparent. The viscosity of the dispersions with the micrographs showing the least defects is too low to be maintained properly. The loss of the shear-thinning functionality is consistent for the use of ionomer IB, which might to be avoided for the use on a larger scale.

3.4.2 Experiment 2: Dissolver and Infrared Dryer

After this first assessment, several process variables are changed for the second trial. The strategy is detailed in Chapter 2.6. The ionomer has been changed to ionomer IA, to avoid the loss of shear-thinning flow, the stirring period has been reduced to 3 h, using the results discussed in Section 3.1, the comminution is changed to a high-speed dissolver to investigate the viability of this elsewhere established method [52 p. 101ff]. The dryer for the CL formation on the decal foil is changed from a convection to an infrared radiation dryer for the same reason. The dispersions are characterized again by AC, the results are presented in Figure S 14. In nuce, the stability is again improved by a stirring period, and the comminution can further increase the stability. Nonetheless, the stability of the samples prepared with the small beads mill is not reached (comp. Figure S 8 d-f). Additionally, the PSDs of the dispersion were determined as well and are displayed in Figure 9a. The distributions are wide, comparable to the samples from the adsorption study (Figure S 3c). Minor changes are apparent as the distribution is no longer bimodal but monomodal, indicating a large portion of larger agglomerates. The comminution, however, does only marginally change the broad PSDs such that the smaller particles are more numerous. The viscosity was determined as well (Figure 9b). The flow curves show a partial repetition of the results on the smaller scale (Figure 7c). The viscosity does not change much for the dispersion without the stirring period but the dispersions with the 3 h stirring period can be subject to changed flow behavior. However, a clear trend does not emerge from this, which complicates predictions. In any case, the dispersions did not run-off during the application in the coating step.

The micrographs displayed in Figure S 15 and Figure S 16 show the formation of large agglomerates (50 – 200 µm), clearly indicating the insufficiency of the dissolver as a tool for

comminution in this use case. However, despite the large agglomerates, the typical cracks next to the agglomerates are not apparent. This is likely due to the change from a convection or conduction dryer to a radiation dryer. The faster, intensified drying limits the movement of liquids along the coating [12], which reduces the capillary pressure and thereby the formation of cracks as a result of the coating yielding to the internal stress.

In summary, the results show that the dissolver is not suited for the comminution task and should be avoided. It is possible that a much longer operation period would improve the results, however comminution operations in general have a high demand of electrical energy, thus that hours-long operations cannot be favored over minutes-long. On the other hand, the use of the infrared dryer reduced the formation of defects even under adverse circumstances.

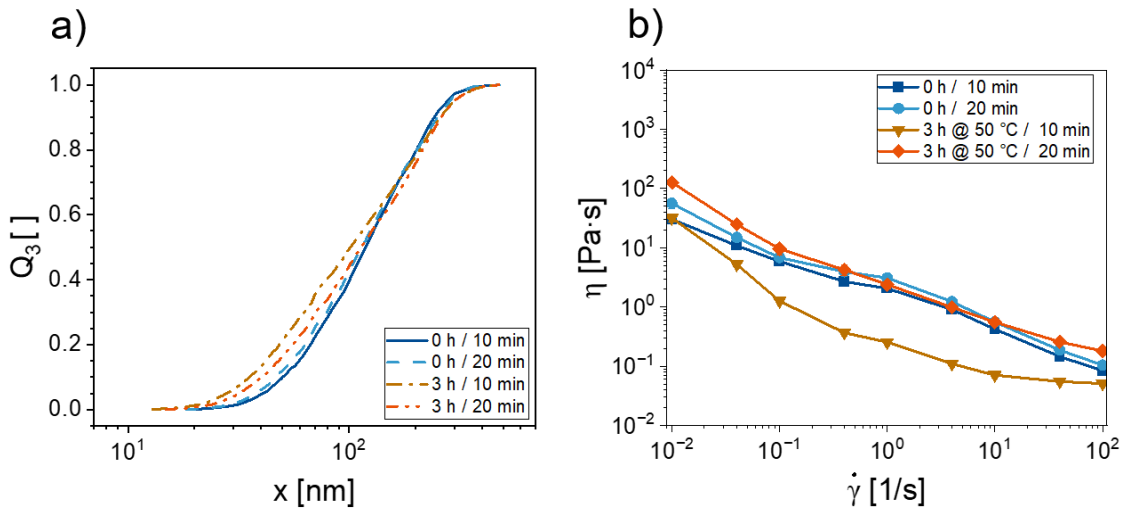

Figure 9 Dispersion characterization of catalyst dispersions from for the pilot scale experiment 2 prepared with the dissolver. The first number of the sample labeling referrers to the stirring duration in hours, the second to the comminution duration in minutes. a) PSDs and b) flow curves of dispersions.

3.4.3 Experiment 3: Filmix and Infrared Dryer

Following the results of all experiments above, the process variables have been chosen. Comparing the dispersion formulation, ionomer IA is preferable over IB, for yielding shear-thinning dispersions. The stirring period of 3 h at 50 °C is sufficient and was used again. The comminution with the dissolver was not successful, so the Filmix was used to comminute for 5 min. The infrared drying was favorable to cure the CL. Only a single batch has been produced without further variations. All the results of this final approach are summarized in Figure 10. The transmittogram (a) ascribes a reasonable stability of the dispersion against sedimentation, which is better than any other results on pilot scale in this work. The PSD (b) is narrow and similar to the results achieved on smaller scale (comp. Figure 7a and [12]). The flow curve shows a shear-thinning behavior with a smaller viscosity as the dispersions prepared with the dissolver, but still high enough to not show any run-off problems during the coating step. The resulting CLs show a limited formation of agglomerates (< 100 µm), but without any defects like cracks or pinholes detectable.

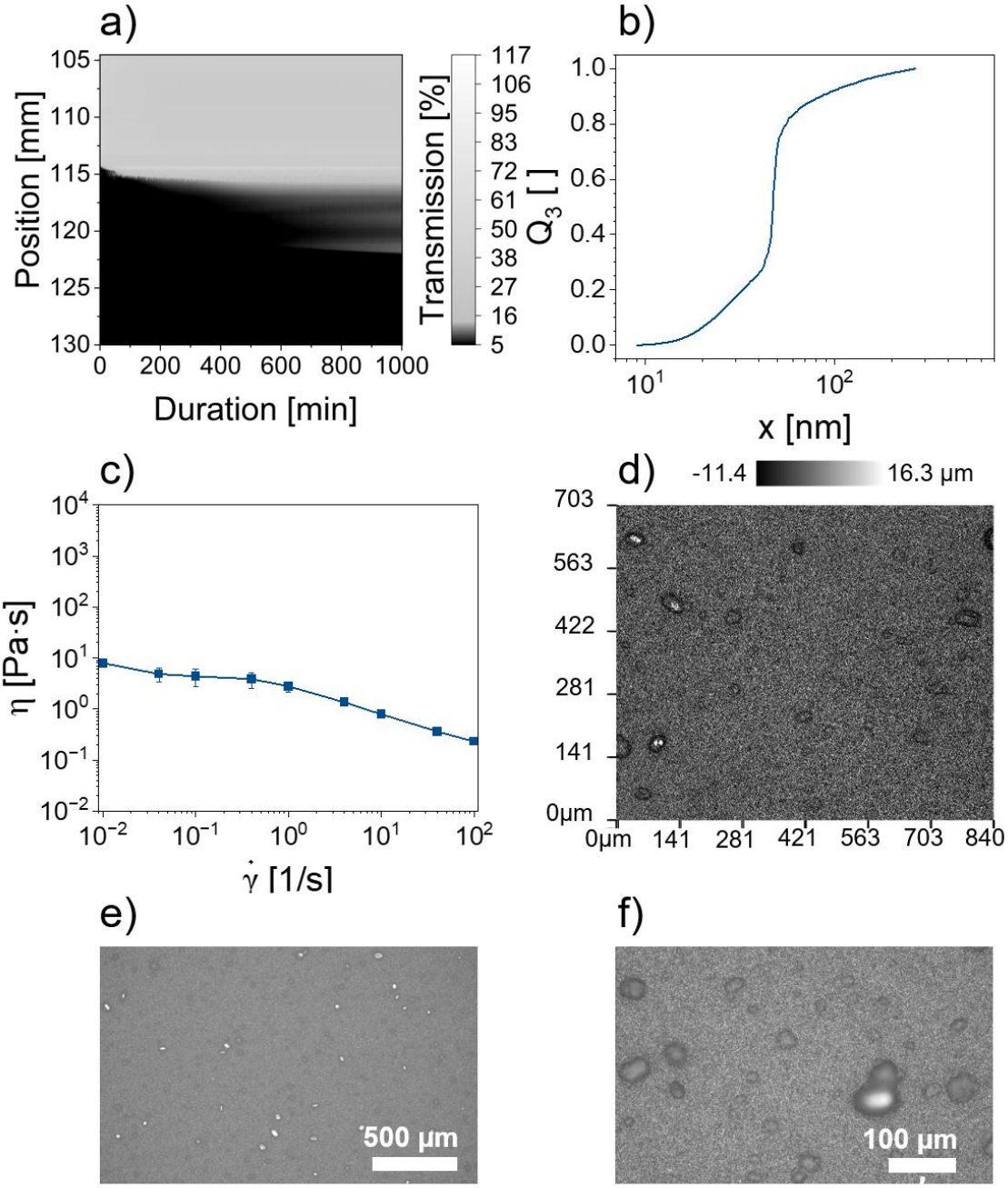

Figure 10 Dispersion and layer characterization of catalyst dispersions from for the large batch Experiment 3 prepared with the Filmix. a) Transmittogram, b) PSD by AC and c) flow curve of the dispersion; CL characterization by d) optical profilometry, e) and f) optical microscopy.

3.4.4 Concluding remarks

These experiments from perspective of the catalyst dispersion and layer on decal foil as semifinished goods lead in summary to the recommendation of the following process variables:

- For the ionomer, IB cannot be recommended, since it either yields a dispersion with large agglomerates (without stirring) or a very low viscosity causing run-off problems (with stirring). It is therefore necessary to test the flow behavior of the ionomer beforehand and select according to it.
- For the comminution operation, the Filmix rotor-stator is to be preferred over the dissolver. The shear forces induced by the latter do not seem to be sufficient to break up larger agglomerates.
- The infrared radiation dryer appears to be advantageous over the convection dryer, as lesser defects are produced and the length of the operation in the R2R plant is reduced by about a third.

3.5 Electrochemical performance evaluation

Finally, to evaluate the quality of the most promising CLs prepared in Chapter 3.3 and 3.4 the electrochemical performance was tested using a test full-cell setup with realistic conditions as described in [12]. These CLs were selected for their representative quality – which is not necessarily an ideal defect-free layer – for the respective fabrication method. The CLs are:

- From 3.3 on small scale (4 CLs):
  - Ionomer IA without stirring, 20 min beads milling
  - Ionomer IA with 24 h stirring, 20 min beads milling
  - Ionomer IB without stirring, 20 min beads milling
  - Ionomer IB with 24 h stirring, 20 min beads milling
- From 3.4 on large scale (5 CLs):
  - Ionomer IB with 24 h stirring, 1 min Filmix, convection drying
  - Ionomer IB with 24 h stirring, 5 min Filmix, convection drying
  - Ionomer IB without stirring, 5 min Filmix, convection drying
  - Ionomer IA with 3 h stirring, 20 min dissolver, infrared drying
  - Ionomer IA with 3 h stirring, 5 min Filmix, infrared drying

The polarization curves, which is the characteristic curve under constant conditions for each catalyst layer, are presented in Figure 11. To achieve high electrical power output, the fuel cell should maintain a high cell voltage U_{cell} at a given current density i, resulting in a higher power density. This enables a reduction in the required active area and consequently decreases the catalyst demand for a given stack power output. As all samples are prepared with the same nominal wet film thickness and concentration, the catalyst content is supposed to be the same for every catalyst layer. Additionally, cyclic voltammetry has been performed (Figure S 17). The results correlate well with the polarization curves.

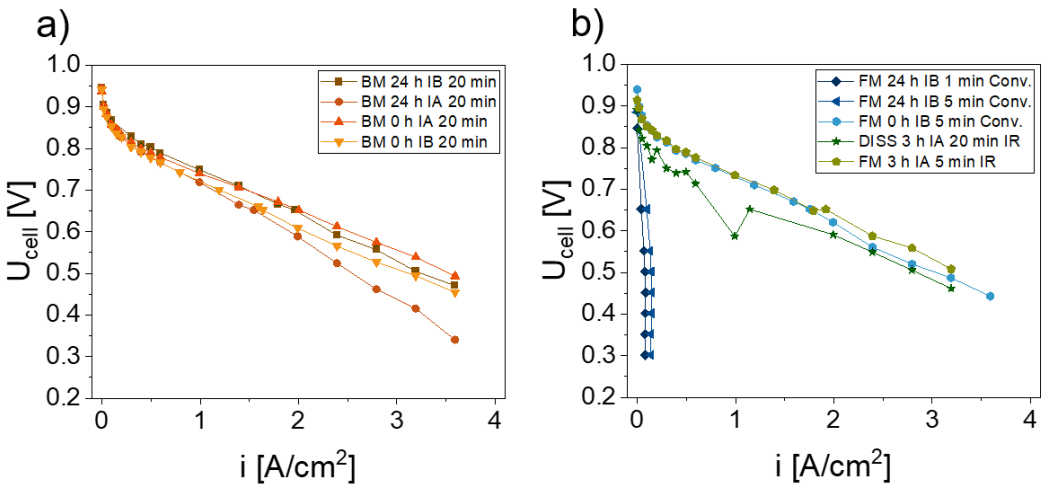

Figure 11 Polarization curves for performance evaluation of the catalyst layers. a) catalyst layers from lab-scale table-top coating, b) catalyst layers prepared on pilot scale. BM: lab scale beads milling, FM: pilot scale Filmix, DISS: dissolver; time in h refers to the stirring period at 50 °C; the time in min to the comminution; Conv.: convection drying at 80 °C, IR: infrared drying at 90 °C.

Figure 11a) shows the performance of the catalyst layers prepared on laboratory scale with the table-top coating machine. Here, coatings are prepared with dispersions from beads milling with different times for stirring as well as different ionomers. All the samples show a rather high performance with some differences in the high current-density regime where e.g. transport losses become apparent. However, the differences are very large. The samples prepared with ionomer IA show a higher performance for the samples without stirring, with IB it is vice versa. As seen in Figure S 9 and Figure S 10, the sample with IA, 24 h stirring and 20 min comminution seems to have lost some material which got loose from the CL. The sample shows an onset of mass transport limitations at lower cell voltages, which may be due to the loss of catalyst as well as a possibly less optimal optimal pore network. In Chapter 3.3 it was apparent that the viscosity is the major difference between the dispersions. However, on a laboratory scale with leverled table-top coating equipment, the different viscosities do not result in different performance. This is not the case for the samples prepared on pilot scale.

In Figure 11b) the polarization curves of the catalyst layers prepared with pilot scale methods are presented. It is apparent that two of the curves show only a poor performance. These two are from the first set of pilot scale coatings, prepared with ionomer IB and the 24 h stirring time. However, the sample prepared with IB but without the stirring time (“0 h”) has a reasonably high performance. The difference between these samples is the viscosity. While the sample without the 24 h stirring period (“0 h”) has a rather high viscosity, the prestirred samples have a very low viscosity facing run-off problems, as the liquid catalyst dispersion runs retrograde to the web out of the coating unit. This results in very thin coatings, insufficient for the high performance demands in a PEM-FC application and with the possible danger to leak hydrogen. The other two layers prepared on larger scale are prepared with ionomer IA and did not have any run-off problems. The larger agglomerates of the layer from the second larger experiment with the dissolver are likely to lower the performance compared to the two better performing layers, as the catalyst within these agglomerates face higher transport hinderance. Furthermore, the scattering of the measurement is likely due to the uneven layer

as well. The catalyst layer from the third pilot scale experiment shows a reasonably high performance similar to the best layer from the first experiment. Overall, the performance falls just short from the best layers on lab-scale (Figure 11a, [12]).

4. Conclusions

In this work, key aspects of the catalyst dispersion and layer formation for the preparation of catalyst coated membranes for hydrogen fuel cells are investigated. The study aims to fulfil certain quality demands on the catalyst dispersion, layer formation and untimely performance. This was done following the process scheme in Figure 1 and investigating the process variables. Throughout this work it became increasingly apparent that these quality demands are not necessarily met simultaneously. For example, from the first set of pilot scale experiments the best performance was by a CL from an unstable dispersion and a layer with drying induced cracks due to larger agglomerates. This means, the demands on dispersion, layer formation and performance need to be investigated and evaluated independently. This is even true for the viscosity, since the flow properties have an impact on the layer formation, however even viscous dispersions can be unstable to sedimentation. In other words: a promising dispersion or catalyst layer are not a guarantee for high performance, or vice versa. The frame for meeting all demands simultaneously seems narrow.

For the scaling of the dispersion preparation, the adsorption kinetics of the ionomer have been investigated since the adsorption has a large impact on the catalyst dispersion stability and viscosity. The gravimetric methodology is not very precise, however it is versatile, and trends can be identified. For the two investigated ionomers it was found that moderate 50 °C is optimal for the dispersion preparation, as a higher temperature triggers gelation and a lower temperature limits the adsorption process. For this temperature, 3 h agitation time has been found to be sufficient, drastically reducing the formerly used 24 h stirring overnight. This enables the scaled production of catalyst dispersions on a reasonable time scale.

To further facilitate the scaling of the stirring process step, the workflow has been investigated briefly in a proper setup. Here, it was found that the chemicals cannot be added in arbitrary order, but the catalyst powder needs to be added the latest into a wetting liquid under agitation. Since the polymer often arrives as a dry powder, it should be dissolved carefully into the water alcohol mixture first. After all chemicals have been added, the dispersion can be heated to the suggested temperature. Furthermore, the agitation mechanic was investigated with different agitator geometries. Here, classical approaches with dimensionless numbers are applicable, adjusted by the Rieger-Novák procedure for shear-thinning fluids. However, the dynamic behavior of the ionomer, i.e. adsorption, and the change in viscosity cannot be considered by these methods and have to be evaluated carefully. Since the agitator needs to provide axial flow for a wide range of viscosity, the helical ribbon was found to be the most promising. It also requires the least power density. With these experiments and the provided scale-up criteria the agitation can readily be used in production scale what can be seen as a major step forward with regard to methods-development for CCM production. Since the complex behavior of the ionomers, the absolute powder demand should be designed conservatively.

The comminution however seems to be more difficult to evaluate. Therefore, not only the catalyst dispersion but also the resulting CLs on the transfer foil are used as a measure to evaluate the viability of different methods. Beads milling was applied on a smaller laboratory scale. Here it was found that the dispersion properties depend strongly on if it was stirred at 50 °C before comminution, depending on the ionomer. The performance, however, is independent from the viscosity due to the use of a levelled lab-scale table-top coater, as it is common to use.

On a pilot scale however, the viscosity is an important factor. As the substrate is moved on roll through the coating section with the commabar, the liquid tends to run off if the viscosity is too low. The limit can be found to be about 1 Pa·s at 0.1 1/s. If the viscosity is much lower (e.g. 0.1 Pa·s), the dispersion is likely to face run off, if it is much higher (e.g. 10 Pa·s), it is avoided. Major leveling problems have not been found for dispersions of this viscosity.

The pilot scale experiment showed that proper comminution and agitation is necessary to provide both layers with as few defects as possible and high electrochemical performance. Here the Filmix rotor-stator system with a high-speed rotor and a narrow shear gap as well as the use of radiation dryers such es infrared radiation can be recommended. In any case, the ionomer behavior should be investigated beforehand, such that the dispersion is stable and medium viscous, and the ionomer does not lower the viscosity of the dispersion too much during adsorption.

To conclude, this work provides vital insights for the scaled fabrication of CCMs by the indirect process route, starting from the process variables for the dispersion agitation and comminution and finalizing with the layer formation and performance on pilot scale.

Acknowledgments

Financial support of this work by the Ministry of Economic Affairs, Industry, Climate Action and Energy of the State of North Rhine-Westphalia with the project R2R-CCM is gratefully acknowledged. The authors would also like to thank the collaboration partners Hydrogen and Fuel Cell Center (ZBT) and Laufenberg GmbH for considerable experimental support and the Interdisciplinary Center for Analytics on the Nanoscale (ICAN) for analytical measurements. DS thanks the Mat4Hy consortium for cooperation.

Data availability

Data is available on Nomad-Lab. DOI: XX.XXXXX/NOMAD/2026.XX.XX-X

References

1. B. James, J. Huya-Kouadio, C. Houchins and M. Gomez, *Mass Production Cost Estimation of Direct H_2 PEM Fuel Cell Systems for Transportation Applications (2017 - 2021) (Final Report) (*2021).
2. A. Willert, F. Z. Tabary, T. Zubkova, P. E. Santangelo, M. Romagnoli and R. R. Baumann, *Acta Physicochim URSS,* **47**(48), 20973–20986 (2022), 10.1016/j.ijhydene.2022.04.197.
3. C. A. Gomes Bezerra, L. J. Deiner and G. Tremiliosi-Filho, *Adv Eng Mater,* **21**(11) (2019), 10.1002/adem.201900703.
4. B. Millington, V. Whipple and B. G. Pollet, *Journal of Power Sources,* **196**(20), 8500–8508 (2011), 10.1016/j.jpowsour.2011.06.024.
5. Y. Zhu, M.-A. Kräenbring, I. Radev, A. S. Odungat, L. Grebener, O. Pasdag, T. B. Nguyen, D. Segets and F. Özcan, *Energy Adv.,* **5**(4), 434–447 (2026), 10.1039/d5ya00372e.
6. S. A. Mauger, K. C. Neyerlin, A. C. Yang-Neyerlin, K. L. More and M. Ulsh, *J. Electrochem. Soc.,* **165**(11), F1012-F1018 (2018), 10.1149/2.0091813jes.
7. J. Sharma, X. Lyu, T. Reshetenko, G. Polizos, K. Livingston, J. Li, D. L. Wood and A. Serov, *Acta Physicochim URSS,* **47**(84), 35838–35850 (2022), 10.1016/j.ijhydene.2022.08.157.
8. A. Burdzik, M. Stähler, I. Friedrich, M. Carmo and D. Stolten, *Journal of Coatings Technology and Research,* **15**(6), 1423–1432 (2018), 10.1007/s11998-018-0074-3.
9. J. Park, Z. Kang, G. Bender, M. Ulsh and S. A. Mauger, *Journal of Power Sources,* **479,** 228819 (2020), 10.1016/j.jpowsour.2020.228819.
10. M. Bodner, H. R. García, T. Steenberg, C. Terkelsen, S. M. Alfaro, G. S. Avcioglu, A. Vassiliev, S. Primdahl and H. A. Hjuler, *Acta Physicochim URSS,* **44**(25), 12793–12801 (2019), 10.1016/j.ijhydene.2018.11.091.
11. W. Pan, Z. Chen, X. Chen, F. Wang and G. Dai, *AIChE Journal,* **68**(8), e17719 (2022), 10.1002/aic.17719.
12. L. Grebener, A. S. Odungat, Y. Zhu, O. Pasdag, I. Radev, E. Nürenberg, A. Kubina, V. Peinecke, S. Kohsakowski, D. Segets and F. Özcan, *Journal of Power Sources,* **635,** 236457 (2025), 10.1016/j.jpowsour.2025.236457.
13. A. S. Odungat, L. Grebener, O. Pasdag, T. B. Nguyen, Y. Zhu, S. Kohsakowski, I. Radev, F. Özcan and D. Segets, *Adv Energy and Sustain Res (*2025), 10.1002/aesr.202500043.
14. Y. Guo, D. Yang, B. Li, D. Yang, P. Ming and C. Zhang, *ACS Applied Materials & Interfaces,* **13**(23), 27119–27128 (2021), 10.1021/acsami.1c07070.
15. S. H. Woo, S. Kim, S. Woo, S.-H. Park, Y. S. Kang, N. Jung and S.-D. Yim, *Korean J. Chem. Eng.,* **40**(10), 2455–2462 (2023), 10.1007/s11814-023-1474-3.
16. G. Doo, J. H. Lee, S. Yuk, S. Choi, D.-H. Lee, D. W. Lee, H. G. Kim, S. H. Kwon, S. G. Lee and H.-T. Kim, *ACS Applied Materials & Interfaces,* **10**(21), 17835–17841 (2018), 10.1021/acsami.8b01751.
17. R. Sharma and S. M. Andersen, *ACS Applied Materials & Interfaces,* **10**(44), 38125–38133 (2018), 10.1021/acsami.8b14622.
18. H. Liu, L. Ney, N. Zamel and X. Li, *Applied Sciences,* **12**(8), 3776 (2022), 10.3390/app12083776.
19. W. Yoshimune and M. Harada, *bull. Chem. Soc. Jpn.,* **93**(2), 302–307 (2020), 10.1246/bcsj.20190321.

20. M. Chisaka, E. Matsuoka and H. Daiguji, *J. Electrochem. Soc.,* **157**(8), B1218 (2010), 10.1149/1.3439617.
21. M. B. Dixit, B. A. Harkey, F. Shen and K. B. Hatzell, *J. Electrochem. Soc.,* **165**(5), F264-F271 (2018), 10.1149/2.0191805jes.
22. S. MA, Q. CHEN, F. JOGENSEN, P. STEIN and E. SKOU, *Solid State Ionics,* **178**(29-30), 1568–1575 (2007), 10.1016/j.ssi.2007.10.007.
23. H. Mizukawa and M. Kawaguchi, *Langmuir,* **25**(20), 11984–11987 (2009), 10.1021/la9025188.
24. S.-J. Shina, J.-K. Lee, H.-Y. Ha, S.-A. Hong, H.-S. Chun and I.-H. Oh, *Journal of Power Sources,* **106,** 146–152 (2002).
25. J. H. Lee, G. Doo, S. H. Kwon, S. Choi, H.-T. Kim and S. G. Lee, *Sci Rep,* **8**(1), 10739 (2018), 10.1038/s41598-018-28779-y.
26. S. Shukla, S. Bhattacharjee, A. Z. Weber and M. Secanell, *J. Electrochem. Soc.,* **164**(6), F600-F609 (2017), 10.1149/2.0961706jes.
27. M. Thoma, W. Lin, E. Hoffmann, M.-M. Sattes, D. Segets, C. Damm and W. Peukert, *Langmuir,* **34**(41), 12324–12334 (2018), 10.1021/acs.langmuir.8b02726.
28. *Ullmann's Chemical engineering and plant design*, Weinheim, Wiley-VCH (2004).
29. A. S. Amin, A. Caidi, T. Lange, I. Radev, D. J. S. Sandbeck, W. Philippi, M.-A. Kräenbring, M. Öztürk, V. Peinecke, D. Lerche, F. Özcan and D. Segets, *Part & Part Syst Charact,* **42**(1) (2025), 10.1002/ppsc.202400069.
30. S. Bapat, C. Giehl, S. Kohsakowski, V. Peinecke, M. Schäffler and D. Segets, *Advanced Powder Technology,* **32**(10), 3845–3859 (2021), 10.1016/j.apt.2021.08.030.
31. S. Bapat and D. Segets, *ACS Appl. Nano Mater.,* **3**(8), 7384–7391 (2020), 10.1021/acsanm.0c01467.
32. S. Rajupet, A. Z. Weber and C. J. Radke, *ACS Applied Materials & Interfaces (*2025), 10.1021/acsami.5c00211.
33. A. S. Amin, D. Lerche, A. S. Odungat, S. U. Boehm, T. Koch, F. Özcan and D. Segets, *ChemCatChem,* **16**(6) (2024), 10.1002/cctc.202301393.
34. R. Sharma, L. Grahl-Madsen and S. M. Andersen, *Materials Chemistry and Physics,* **226,** 66–72 (2019), 10.1016/j.matchemphys.2019.01.015.
35. P. Quarz, N. Zimmerer, P. Scharfer and W. Schabel, *Fuel Cells,* **24**(2), 108–121 (2024), 10.1002/fuce.202300252.
36. N. Kumano, K. Kudo, Y. Akimoto, M. Ishii and H. Nakamura, *Carbon,* **169,** 429–439 (2020), 10.1016/j.carbon.2020.07.047.
37. R. Devivaraprasad and T. Masuda, *Langmuir,* **36**(46), 13793–13798 (2020), 10.1021/acs.langmuir.0c02023.
38. S. M. Andersen, M. Borghei, R. Dhiman, V. Ruiz, E. Kauppinen and E. Skou, *The Journal of Physical Chemistry C,* **118**(20), 10814–10823 (2014), 10.1021/jp501088d.
39. W. Yoshimune and M. Harada, *Chem. Lett.,* **48**(5), 487–490 (2019), 10.1246/cl.190017.
40. R.-L. Tseng, F.-C. Wu and R.-S. Juang, *Journal of the Taiwan Institute of Chemical Engineers,* **41**(6), 661–669 (2010), 10.1016/j.jtice.2010.01.014.
41. J. Wang and X. Guo, *Journal of hazardous materials,* **390,** 122156 (2020), 10.1016/j.jhazmat.2020.122156.
42. P. J. Dudenas and A. Kusoglu, *Macromolecules,* **52**(20), 7779–7785 (2019),

10.1021/acs.macromol.9b01024.
43. S. A. Berlinger, P. J. Dudenas, A. Bird, X. Chen, G. Freychet, B. D. McCloskey, A. Kusoglu and A. Z. Weber, *ACS Appl. Polym. Mater.,* **2**(12), 5824–5834 (2020), 10.1021/acsapm.0c01076.
44. K. B. Hatzell, M. B. Dixit, S. A. Berlinger and A. Z. Weber, *J. Mater. Chem. A,* **5**(39), 20527–20533 (2017), 10.1039/C7TA07255D.
45. M. Zlokarnik, *Stirring: Theory and Practice,* Wiley (2001).
46. A. B. Metzner and R. E. Otto, *AIChE Journal,* **3**(1), 3–10 (1957), 10.1002/aic.690030103.
47. F. Rieger and V. Novák, *Chemical Engineering Science,* **29**(11), 2229–2234 (1974), 10.1016/0009-2509(74)80031-X.
48. Densities and Viscosities of 1-Propanol-Water Mixtures, *JOURNAL OF CHEMICAL AND ENGINEERING DATA,* **Vol. 8**(No. 3) (1963).
49. A. Kusoglu and A. Z. Weber, *Chemical Reviews,* **117**(3), 987–1104 (2017), 10.1021/acs.chemrev.6b00159.
50. W. P. Lee and A. F. Routh, *Langmuir,* **20**(23), 9885–9888 (2004), 10.1021/la049020v.
51. K. B. Singh and M. S. Tirumkudulu, *Physical review letters,* **98**(21), 218302 (2007), 10.1103/PhysRevLett.98.218302.
52. J. Winkler, *Dispergieren von Pigmenten und Füllstoffen*, Hannover, Vincentz Network (2014).

SI content headlines (for referencing in text)

Figure S 1 Correlation of ionomer concentration and dispersion density in water-alcohol without particles. The samples for this correlation have been prepared by mixing the water, alcohol, and the commercial ionomer stock solution.

Figure S 2 Viscosity of catalyst dispersions stirred for 0.5 to 2 h at 30 to 70 °C. The “0 h” sample is prepared by just mixing the components for 5 min at room temperature to provide an initial flow curve. a) dispersions prepared with ionomer IA; b) prepared with IB.

Figure S 3 Cumulative PSD of the catalyst particles by Stokes sedimentation for the catalyst dispersions stirred at for different times at temperatures between 30 and 70 °C. The samples were diluted from 15 wt% to 0.2 wt% before centrifugation. a+c+e) Dispersions with IA prepared at 30, 50, and 70 °C; b+d+f) IB at 30, 50, and 70 °C.

Figure S 4 Transmittograms for the catalyst dispersions prepared by stirring with IA for 30 and 50 °C. 70°C was prepared but not recorded due to the very high viscosity. a) catalyst dispersion with IA, prepared by just 5 min mixing at room temperature; b+d) stirred at 30 °C; c+e) at 50 °C.

Figure S 5 Transmittograms for the catalyst dispersions prepared by stirring with IB for 30 to 70 °C. a) catalyst dispersion with IB, prepared by just 5 min mixing at room temperature; b+e) stirred at 30 °C; c+f) at 50 °C; d+g) at 70 °C.

Figure S 6 Failed wetting and submersion of CB into water. a) at Re = 2000, b) at Re = 5000, c) at Re = 6000 and d) dry CB floating on top of water after stirring.

Figure S 7 Flow curve of the dispersion with CB on logarithmic scale to test for power law.

Figure S 8 Transmittograms of catalyst dispersions after different stirring and comminution durations. The first number referrers to the stirring duration in hours, the second to the comminution duration in minutes in the form of beads milling. a-f) Formulations with ionomer IA, g-l) with IB.

Figure S 9 Micrographs from optical microscopy of catalyst dispersions after different stirring and comminution durations cast onto decal foil. The first number referrers to the stirring duration in hours, the second to the comminution duration in minutes in the form of beads milling. a-f) Formulations with ionomer IA, g-l) with IB.

Figure S 10 Micrographs from optical profilometry of catalyst dispersions after different stirring and comminution durations cast onto decal foil. The first number referrers to the stirring duration in hours, the second to the comminution duration in minutes in the form of beads milling. a-f) Formulations with ionomer IA, g-l) with IB.

Figure S 11 Transmittograms of catalyst dispersions of the first experiments on pilot scale. The first number referrers to the stirring duration in hours, the second to the comminution duration in minutes with the Filmix.

Figure S 12 Micrographs from optical microscopy of catalyst dispersions after different stirring and comminution durations cast onto decal foil prepared in the first set of experiments on pilot scale. The first number referrers to the stirring duration in hours, the second to the comminution duration in minutes with the Filmix.

Figure S 13 Micrographs from optical profilometry of catalyst dispersions after different stirring and comminution durations cast onto decal foil prepared in the first set of experiments on pilot scale. The first number referrers to the stirring duration in hours, the second to the comminution duration in minutes with the Filmix.

Figure S 14 Transmittograms of catalyst dispersions of the second experiments on pilot scale. The first number referrers to the stirring duration in hours, the second to the comminution duration in minutes with the dissolver.

Figure S 15 Micrographs from optical microscopy of catalyst dispersions after different stirring and comminution durations cast onto decal foil prepared in the second set of experiments on pilot scale. The first number referrers to the stirring duration in hours, the second to the comminution duration in minutes with the dissolver.

Figure S 16 Micrographs from optical profilometry of catalyst dispersions after different stirring and comminution durations cast onto decal foil prepared in the second set of experiments on pilot scale. The first number referrers to the stirring duration in hours, the second to the comminution duration in minutes with the dissolver.

Figure S 17 Cyclic voltammetry for performance evaluation of the catalyst layers by ZBT. a) catalyst layers from lab-scale table-top coating, b+c) catalyst layers prepared on pilot scale. BM: lab scale beads milling, FM: pilot scale Filmix, DISS: dissolver; time in h refers to the stirring period at 50 °C; the time in min to the comminution; Conv.: convection drying at 80 °C, IR: infrared drying at 90 °C**.**